Optical Beam Steering with Focus Tunable Lenses for Automotive LIDAR Systems

Lamia Siddiquee

A Thesis

In the Department

of

Electrical and Computer Engineering

Presented in Partial Fulfillment of the Requirements

for the Degree of Master of Applied Science at

Concordia University

Montreal, Quebec, Canada

December, 2018

CONCORDIA UNIVERSITY
SCHOOL OF GRADUATE STUDIES

This is to certify that the thesis prepared

By: **Lamia Siddiquee**

Entitled: **Optical Beam Steering with Focus Tunable Lenses for Automotive LIDAR Systems**

and submitted in partial fulfillment of the requirements for the degree of

Master of Applied Science

Complies with the regulations of this University and meets the accepted standards with respect to originality and quality.

Signed by the final examining committee:

_____ Chair
Dr. Wen-Fang Xie

_____ Examiner, External
Dr. Wen-Fang Xie To the Program

_____ Examiner
Dr. Krzysztof Skonieczny

_____ Supervisor
Dr. John Xiupu Zhang

Approved by: _____
Dr. W. E. Lynch, Chair
Department of Electrical and Computer Engineering

_____20_____

_____
Dr. Amir Asif, Dean
Gina Cody School of Engineering and
Computer Science

ABSTRACT

Optical Beam Steering with Focus Tunable Lenses for Automotive LIDAR Systems

Lamia Siddiquee

LIDAR is a device used for measuring the distance of an object using laser beams to create detailed 3-D images of the object. LIDAR has numerous applications, but one of its principle applications recently has been with autonomous vehicle where it is used to map the surroundings of the vehicle so that it can detect obstacles or differentiate between roads, other vehicles and passengers etc.

For a LIDAR to capture a complete 360° surrounding view of a vehicle, the sensor must be rotated around to detect images all around the vehicle. Current autonomous cars use spinning LIDAR sensors mounted on top of the vehicle. These sensors use mechanical motors to rotate the entire device, and have the disadvantage of being bulky, expensive, and inefficient. For this reason, non-mechanical methods of steering optical beams like Optical Phased Array (OPA) technology and Micro-electromechanical systems (MEMS) is being extensively researched.

This thesis aims at refining an alternative method of non-mechanical beam steering which uses focus tunable lenses. Focus tunable lenses have a variable focal length that can be controlled by applying appropriate electrical signals. By using two such lenses one after the other, the direction and focus of a laser beam can be controlled. The tunable lenses, along with other optical elements can be used to create a wide-angle scan. Past research on this method is limited, and the device size was too large for practical applications. This can be attributed to the long optical path lengths present between adjacent elements in the design, which is required for the beam scan angle to be

as large as possible. So ultimately a tradeoff between device size and the scan angle exists. This work aims to explore this tradeoff and create a compact design which at the same time is capable of scanning over a large angle. Zemax software was used to model the elements, design the systems, and trace the rays to detect their exact position for different values of focal length of the tunable lenses.

The first design aimed at observing the effect of reducing the optical path length between the adjacent elements in the design. The design elements were placed close to each other to reduce the physical length (and consequently the optical path length) between them. The total length of the device was only 114 mm, but reducing the optical path resulted in a very low scan angle of 16°.

In the second design, instead of removing a big part of the optical path between the relay lens and the diffuser all together, it was replaced with two 90° prisms with their bases facing each other. With this arrangement, a total optical path of 224 mm was created within a physical length of 48mm. The focal length of the objective lenses placed after the diffuser were reduced from 50mm to 25mm. The results from the final design show a total beam scan angle of 52° for a device only 119mm in length.

The third design incorporated a third prism to further increase the optical path length to create a larger scan. The scan angle from this design was found to be 60°. The total size of the device however, increased due to the addition of a third prism.

Measurements were made of the RMS beam radius at different distances from the device, and the beam divergence was calculated to be 0.45°.

ACKNOWLEDGEMENT

I would like to start out by expressing my deepest gratitude towards my supervisor Dr. John Xiupu Zhang for his help and guidance in completing this work.

I would like to thank my parents Dr. Habib Ibrahim Siddiquee and Mrs. Shaila Akhter for their unconditional love and support throughout my life. I would also like to thank my sister Sinchita Siddiquee and my brother-in-law Md. Atai Rabbi for motivating and encouraging me during stressful times.

Finally, I would like to thank all my colleagues at the IPhotonics Laboratory for their help and advice.

TABLE OF CONTENTS

LIST OF FIGURES

LIST OF TABLES

LIST OF ACRONYMS

LIDAR	Light Detection and Ranging
TOF	Time-of-Flight
CW	Continuous Waveform
MEMS	Microelectro-Mechanical Systems
DARPA	Defense Advanced Research Projects Agency
RADAR	Radio Detection and Ranging
OPA	Optical Phased Array
DMD	Digital Micromirror Device
BSDF	Bidirectional Scattering Distribution Function
FOV	Field of View

1. INTRODUCTION

1.1 INTRODUCTION TO LIDAR

The word LIDAR originated from a combination of the words light and radar. The working principle of a LIDAR is quite similar to that of a radar except laser beams are used instead of radio waves. The laser beams emitted from the LIDAR hits the target and reflects back to the LIDAR device, and the total travel time of the laser beam along with its known speed is used to calculate the distance of the target object from the LIDAR device. Using this information, detailed 3-D images of the target can be acquired. [1]

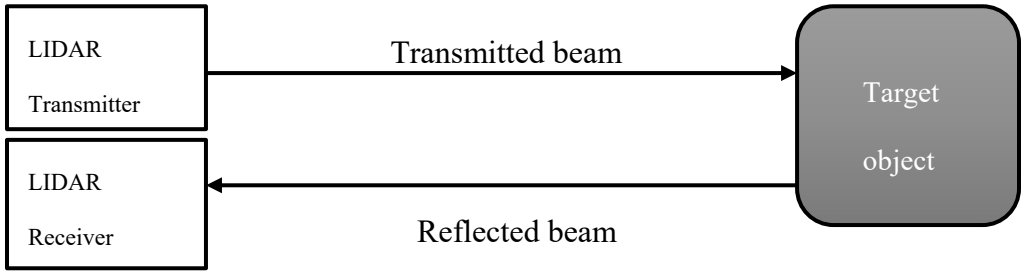

Figure 1.1 Basic working principle of LIDAR

Figure 1.1 above shows the basic working principle of LIDAR. If the distance between the sensor and the object is *d*, the total distance the laser beam travels during the round-trip is therefore *2d*, and if the time taken for the beam to reflect back to the LIDAR device is *t*, then the distance *d* can be found from the formula [14]:

$$d = \frac{c \times t}{2}$$

Where c is the known speed of light.

LIDAR plays an essential role in object detection systems in self-driving cars. Modern self-driving cars use a combination of LIDAR, radar, and camera technology to map detailed images of its surroundings. While cameras are capable of taking high resolution images, they lack the ability to measure distance and velocity of an object. On the other hand, radar measures distance and velocity accurately, but because it uses radio waves it cannot accurately capture finer details especially at greater distances. [22] LIDAR provides a solution to both of these problems: it can measure distance (and also velocity in some cases) and provide high resolution images. LIDAR also works well in various lighting condition. [38]

1.2 TYPES OF LIDAR

LIDAR is composed of two main components: the transmitter which sends out the laser beam and the receiver where the light is reflected back once it hits the object. Depending upon the type of application, the transmitter and receiver can have different properties or working principles that give rise to different types of LIDAR.

1.2.1 FLASH LIDAR VS SCANNING LIDAR

A scanning LIDAR sends out a beam of light onto a single point of the object being detected. The laser beam is then moved around to scan different points of the object. Therefore each point is detected as a pixel and stored in the detector to create a 3-D image of the object.

On the other hand, in a flash LIDAR system the light is instead diffused onto a whole area at once by the transmitter, illuminating an entire scene. The receiver portion consists of 2-dimensional

array of sensors which then detect the light beams coming from different points as individual pixels to create an image. [30]

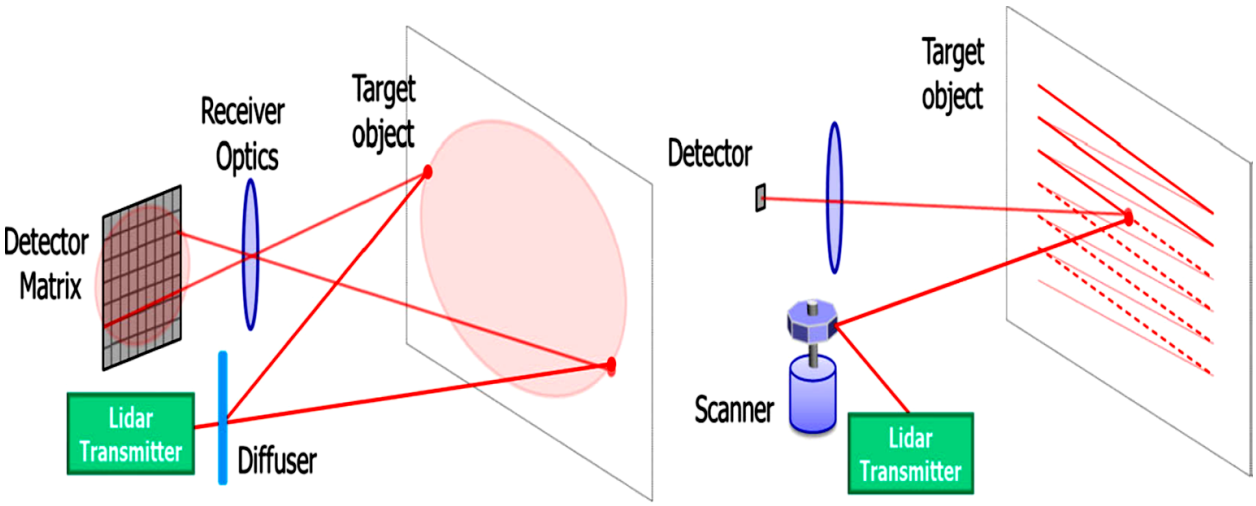

Figure 1.2 Flash LIDAR vs scanning LIDAR [30]

1.2.2 TIME-OF-FLIGHT VS PHASE SHIFT LIDAR

In time-of-flight (TOF) measurement the transmitter sends out pulses of laser and once the light is reflected back to the receiver from the object, the receiver uses the time taken for light to make the round-trip and the known speed of light to measure the distance of the object from the device.

In phase shift measurement, the transmitter consists of a modulated light source, and the receiver calculates the distance of the object based on the phase difference of the transmitted and received light beams. [44]

Limitations are present for both devices either in terms of speed of measurement or the range of distance measured. TOF LIDAR can measure over very long distances but its measurement speed is limited by the speed of light. Since TOF LIDAR can send out one pulse of light at a time, when

detecting objects as far as tens of kilometers the laser pulse can take a long time to make the round trip, thereby decreasing the number of laser pulses that can be sent out per second.

On the other hand, phase shift LIDAR can measure objects much faster, but the drawback here is that the wavelength of the modulated waveform limits the distances it can measure with full accuracy. Phase shift LIDAR also makes the use of continuous waveform (CW) light, which would require much higher amounts of average power to be capable of measuring longer distances, and as such would not be eye-safe to be used for all applications. [32]

1.2.3 COHERENT VS INCOHERENT LIDAR DETECTION

Incoherent detection or direct energy detection systems detect changes in amplitude of the reflected light. [14] In this detection scheme the light transmitted by the LIDAR and reflected from the object hits the detector and causes a voltage change proportional to the intensity of the light. No other signals except the reflected light hits the detector hence the name direct energy detection. [33]

The coherent detection scheme employs optical heterodyne detection. The detector receives the reflected signal from the object as well as a reference signal from a local oscillator that beats at a fixed frequency and is therefore capable of detecting the phase changes in the received signal as well as amplitude changes. Coherent LIDAR can measure the distance of the object as well as its velocity by measuring the Doppler shift in frequency [33]. For this reason, coherent detection is more sensitive and can therefore work with lower values of power than incoherent detection schemes. This greater sensitivity however, comes at a cost of greater system complexity. [15]

1.3 LASER PARAMETER REQUIREMENTS FOR LIDAR

The laser transmitter parameters required by a LIDAR device generally depends on the application for which the device will be used. For applications in self-driving vehicles, scanning LIDAR with a pulsed laser source is most commonly used. [15] The parameters of consideration therefore include the wavelength, beam divergence, average output power, peak output power and pulse repetition rate.

The choice of wavelength can vary between 532 nm to 1550 nm. For applications in Bathymetric (underwater) systems, 532 nm is commonly used because the lowest attenuation is achieved underwater for that wavelength with lower level of backscattering. Airborne applications use wavelengths around 1 μm which costs less and consumes less energy [36], but the maximum power is limited due to safety requirements in this wavelength range. Some applications expand the beam to reduce the safety hazard. The two most popular LIDAR wavelengths used in autonomous vehicle applications are 905 nm and 1550 nm. The main advantage of 905 nm is that silicon absorbs photons at this wavelength so cheaper silicon detectors can be used with 905 nm, while 1550 nm light requires more expensive InGaAs photodiodes. However, 1550 nm is safe for human vision at higher values of power and radiant energy which is an important attribute for autonomous vehicles. Atmospheric conditions, reflectivity of detected objects and particle scattering in the air are all affected by wavelength, which brings some complexity into how wavelength is selected. Generally, attenuation of the signal at 905 nm is lower, whereas 1550 nm is can use higher levels of power which makes it suitable for detecting objects at longer distances. [34] [36]

Pulsed lasers used for LIDAR come in two forms: high energy pulse systems emit high power light waves which are not eye safe, and are primarily used for atmospheric research systems, whereas micro-pulse systems use low powered eye safe laser beams. The lasers in micro-pulse systems

emit beams with energy in the range of micro-joules, with a high repetition rate and this form of laser is used in autonomous vehicles. [15] To be able to measure objects several kilometers away, the peak output power of the laser pulse needs to be in the range of tens or hundreds of Watts. [48] However, pulsed lasers with high repetition rates, and nanosecond level pulse duration can bring down the average power of the laser to eye-safe levels. [49]

The effect of beam divergence on a LIDAR system can be seen in figure 1.3 below. For scanning LIDAR systems where each point in a scene in scanned and stored to create a 3-D image, beams with high divergence can lead to inaccurate detection of objects leading to a loss of finer details in the detected image. Sources with lower beam divergence leads to more accurate and detailed images with better resolution. Beam divergence also limits resolution for objects located further away from the source and ideally a fully collimated beam is required for LIDAR sources, and

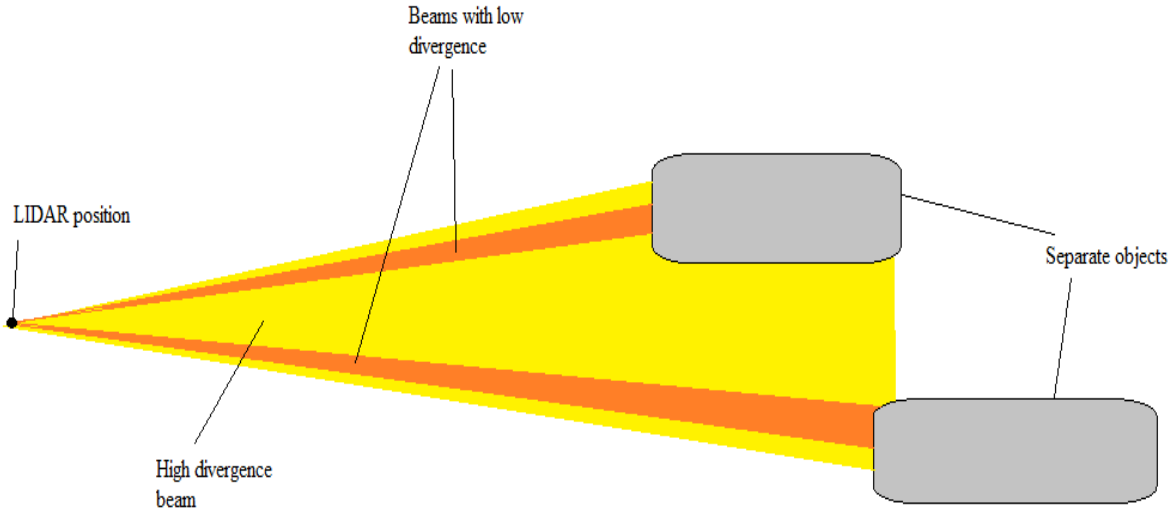

Figure 1.3 Effect of beam divergence in LIDAR

efforts are being made towards making the beam divergence as small as possible in practical devices.

1.4 THESIS OUTLINE:

The rest of the thesis is organized as follows:

Chapter 2 introduces the different methods of steering optical beams and discusses some important work done related to optical beam steering in recent years. The chapter explains how LIDAR is used in autonomous vehicles, and why non-mechanical beam steering methods are essential in creating more effective LIDAR devices. Optical phased arrays and MEMS based scanning systems, which are the most popular technology behind optical beam steering, are discussed in detail. Current progress in optical phased array and MEMS technology is examined and the specifications of each work is presented. The chapter also introduces past work done in optical beam steering using focus tunable lenses, which is the basis of this research.

Chapter 3 discusses the methodology behind the beam steering system of this work. It starts by introducing the principle behind focus tunable lenses and its features. It also talks about the optical design software Zemax which was used to simulate the system. Next, it explains how beam steering is achieved with focus tunable lenses by demonstrating the effect of using one and then two lenses on a beam. The other elements of the system, their features and purpose is discussed next. And finally the various steps of the design process are explained, and the results obtained from each step are displayed. The different design stages are explained, the changes made in the designs and its effect is also presented. Finally, the size, scan angle and beam divergence from each stage is compared.

Chapter 4 concludes the work and summarizes the results achieved from it, and discusses future improvements that can be made.

2. LITERATURE REVIEW

2.1 LIDAR IN AUTONOMOUS VEHICLES

The idea for autonomous vehicles originated as early as 1939 when the General Motors Futarama exhibit at New York World's Fair introduced the idea for radio-controlled self-driving vehicles. But lack of suitable technology hindered sufficient progress to be made towards developing this idea. The research behind self-driving vehicles gained attention again in 2004, when the Defense Advanced Research Projects Agency (DARPA) created it first Grand Challenge, where contestants were promised $1 million for creating an autonomous vehicle that could drive about 150 miles in the Mojave Desert. None of the contestants completed the challenge that year, but the same challenge was completed by 5 contestants in 2005 using improved technology. The technology used, and feats gained by the vehicles in the race stirred interest among major companies like Google to start their own self-driving car research division called Waymo in 2009, followed by other companies like Tesla, General Motors, Toyota, and many more. [22] [15] [24] [25]

Current state of autonomous vehicles is still far from reaching level 5 autonomy, which refers to cars that can travel completely without the help or presence of a human driver. This requires artificial intelligence to gather data from sensors that detect roads, obstacles, traffic lights etc. and process the information to ensure safe operation of the vehicle. Different types of sensors can be used to detect the vehicle's surroundings, and each comes with their own merit. [22]

Both long and short range radar is capable of measuring distance and velocity of moving objects, but falls short in terms of resolution of detected images, and the accuracy due to the longer wavelength of radio waves. Optical cameras on the other hand can capture high resolution images, and can even distinguish between the color of objects making it particularly useful in reading

traffic lights and signals. They cannot however, capture the specific distance of an object or the velocity of moving objects, nor are they reliable in the absence of daylight when they can easily miss a pedestrian walking by. [22]

LIDAR works in similar principle as radar by sending pulses of laser to hit an object and measure its distance by calculating how long it takes for the laser pulse to travel back. The advantage it has over radar is the smaller wavelength of light, which makes LIDAR produce higher resolution images. LIDAR is capable of capturing minor details in scenery more efficiently than even high resolution radar devices (as depicted in figure 2.1 below), which makes them essential in sensing systems of autonomous vehicles. [26] [22]

The ultimate solution is to use all these sensors together to achieve maximum efficiency in the detection of surroundings, so that the benefits of each type of sensor can be utilized.

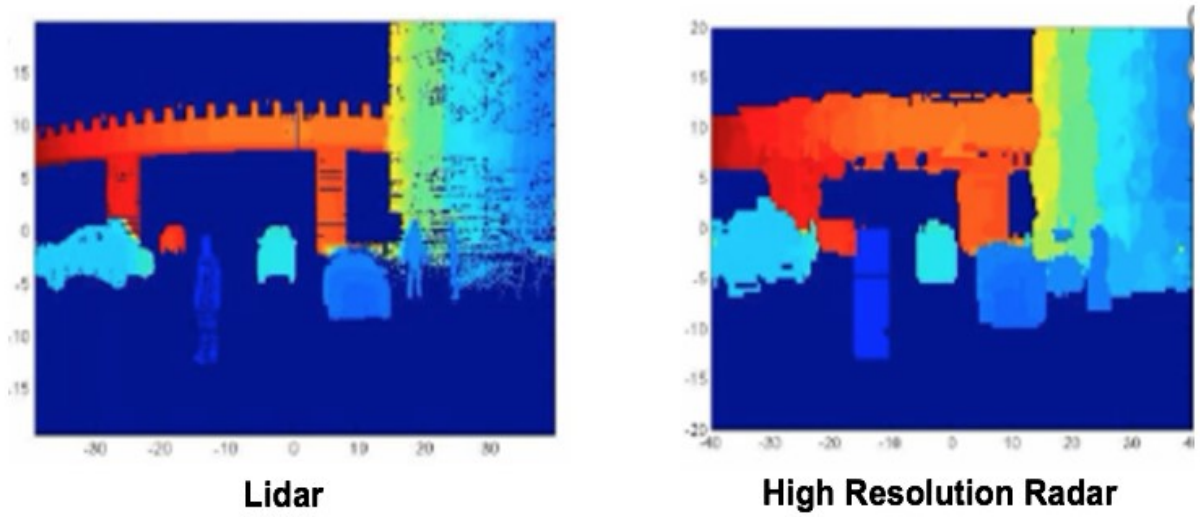

Figure 2.1 Image detail of LIDAR vs high resolution radar [26]

2.2 NEED FOR NON-MECHANICAL BEAM STEERING IN LIDAR

Laser is an essential component of LIDAR systems. Laser beams are fired from the LIDAR and returns to the device which then calculates the time taken for the round trip. The round trip time and the known value for the speed of light can therefore give the precise distance of the object from the LIDAR sensor. This describes one cycle of detection (or one pulse from a pulsed laser source) which gives the data for one point of the object being detected. With the following cycle, the point next to the one previously detected can be mapped, and then the next, and so on. Thus, with a laser source firing thousands of pulses per second, and consequently detecting thousands of different points of an object, a detailed 3-D image of the object can be modeled from the data received. But to detect the different points of the object, the light emitted from the laser needs to be focused on different points on the object. And therefore, the light emitted from the LIDAR transmitter needs to be physically rotated to scan different spots.

Figure 2.2 Velodyne's HDL 64-E spinning LIDAR with a 360° horizontal FOV is extensively used in autonomous vehicles [38]

When it comes to autonomous vehicle applications, a LIDAR transmitter needs to scan the entire 360° surroundings of the vehicle to ensure complete safety of the people inside or outside the vehicle. In current autonomous vehicles, the LIDAR transmitter is perched on top of a mechanical gimbal, and the entire device is mechanically rotated to map the surroundings. Figure 2.3 below shows mechanically steered LIDAR devices mounted on top of self-driving car models by Uber and Google. The need for gimbals and mechanical rotating mechanisms makes these LIDAR devices bulky, expensive and inefficient. In fact, one of the reasons why self-driving cars are too expensive for practical use is because a single LIDAR device could cost up to $60,000. [22]

Figure 2.3 Self-driving vehicles by Uber and Google with spinning LIDAR sensors mounted on top of them. The LIDAR device spins mechanically to capture a 360° view of the vehicle's surroundings [39] [43]

Another consideration for a LIDAR beam scanner is its continuous scanning capability. Continuous scanning plays a major role, particularly for autonomous vehicle systems, as important points in a scan may be missed out with LIDAR systems only capable of scanning discrete points.

In fact, according to [10] high speed continuous beam scanning is more important for such applications than a scanner that can scan in two axes.

2.1.1 OPTICAL PHASED ARRAY

The term phased array refers to the arrangement of individual antennas with controlled phase relationships such that they emit radio waves which combine in a certain way to control the direction of the emitted beam. Each antenna in a phased array is equipped with a phase shifter which is fed with current signals from the transmitter. The current signals determine the phase relationship of the antennas so that the beams they emit combine either constructively of destructively resulting in the emitted beam from the phased array to point in the direction of the greatest constructive interference. This is demonstrated in figure 2.4 below. Phased arrays require individual antennas, with individual phase shifters for each antenna and other controlling electronics. Therefore, there can be thousands of individual elements in a phased array, which makes it impractical for low frequency applications as the device size would be to large. [27]

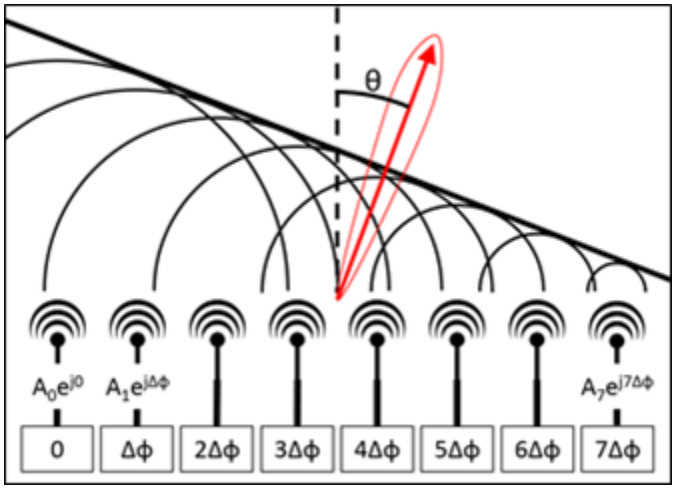

Figure 2.4 Optical phased array principle [37]

Optical phased array (OPA) refers to an arrangement whose purpose is control the direction of an optical beam. Unlike the phased arrays discussed above, the electronics involved in optical phased arrays do not emit the light waves but only control the direction of the light waves produced by a separate laser device. The beam emitted from the laser is split into channels, and the phase of each of these channels is controlled by individual phase tuners to steer the beam into the desired direction. [28]

There have been many different methods used for creating an OPA, some have the drawback of requiring delays to stabilize the device after each scan which greatly slows down the scanning process, especially in the case of continuous scanning [10]. Even with extensive research in the area of optical phased arrays, a major disadvantage in OPA technology is the presence of grating lobes and side lobes. For emitters in an OPA which are which are spaced evenly and greater than half a wavelength apart, grating lobes are generated along with the main lobe which limits the steering angle range. The power emitted between adjacent grating lobes are called side lobes. [29]

Power generated in these lobes travel in different directions than the main lobe causing losses, increasing crosstalk and reducing the efficiency of the device. [10]

Yaacobi et al aimed to tackle some of the issues present in OPA technology in [10] which introduces improvements in wide angle beam scanning using OPA. The optical phased array is fabricated on a 300 µm CMOS compatible platform using silicon based components which limits the device to be only usable for wavelengths above 1.25 µm. It employs cascaded phase shifting architecture with sixteen grating based antennas each 32 µm long, with a 2µm pitch creating a 32 µm × 32 µm array. The device achieved a continuous 1-D scanning angle up to 51° with a maximum steering speed of 5×10^6 deg/sec. However, the 32 µm rectangular aperture results in a considerably large beam divergence of 3.3°. In addition to that there is considerable power loss in the side lobes which makes the device only 25% efficient.

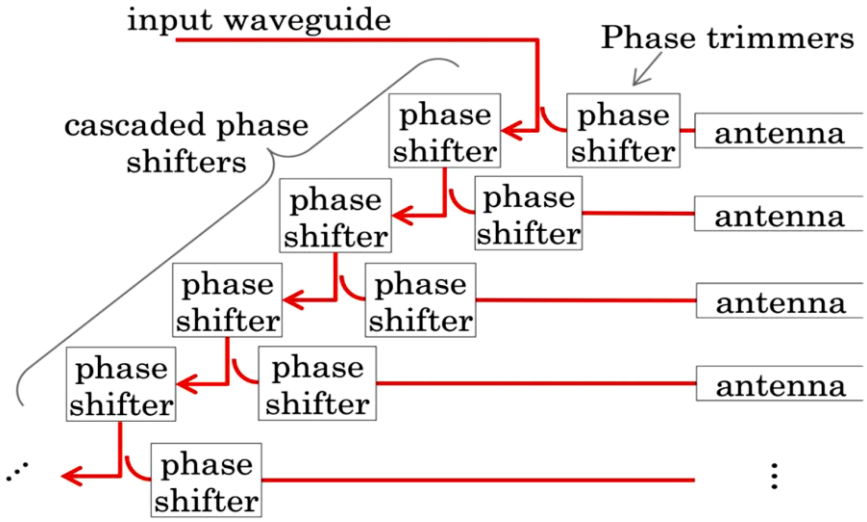

Figure 2.5 Cascaded phase shifting architecture [10]

Poulton et al in [16] suggest an all-in-one LIDAR device with the transmitter, receiver and optical phased array for beam steering integrated into one chip. Similar to the architecture described

above, this device was fabricated on a silicon photonics platform which is CMOS compatible which makes the device only compatible for wavelengths above 1.1 µm. The array is composed of 50 antennas each 500 µm long with a 2 µm pitch. The steering angle range achieved in 2-D was 46°×36° with beam divergence of 0.85° which is considerably smaller than [10]. The power consumption of the device however was high at 1.2 W with high power in the grating lobes along with the main lobe. The maximum range achieved was also limited to 0.5 m by the aperture size.

In an effort to increase the steering angle range of OPA architecture, Hutchison et al [29] proposed a new emitter architecture which uses non-uniform emitter spacing and wide angle emitters to suppress grating lobes which limit the steering angle range in traditional OPA devices. A very wide angle steering range was achieved which was 80° with low divergence of 0.14°. The tradeoff here for high steering range was increased side lobe power.

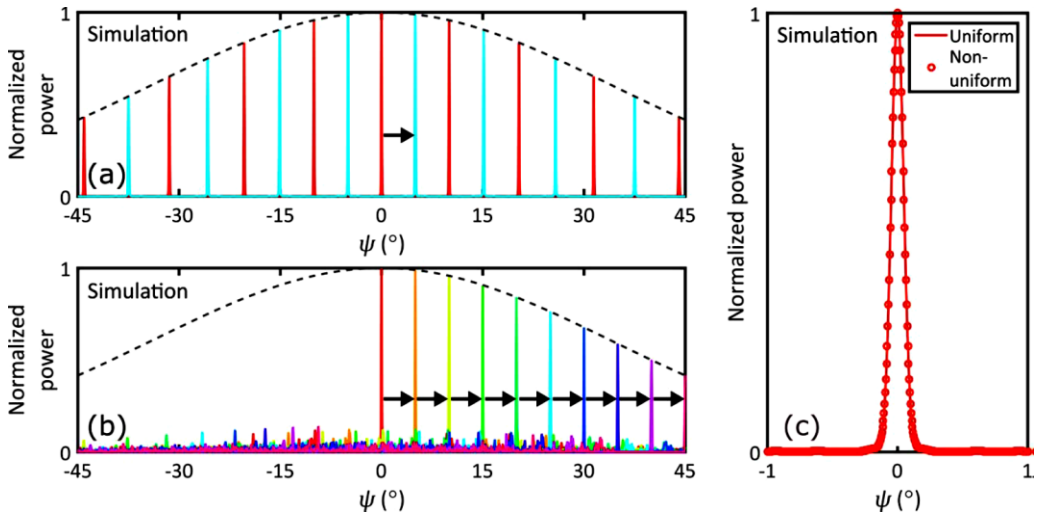

Figure 2.6 Simulation of the OPA from [29] showing beam steering using (a) uniform emitter spacing, and (b) non uniform emitter spacing. The beam is steered to 10 different angles in (b) compared to 2 different angles in (a). Also, there is presence of higher side lobe power in (b). (c) shows a close-up of the main lobe

A fully integrated beam steering chip was proposed by Hulme et al in [2]. The device consisted of 164 optical elements to steer an optical beam emitted from a laser which was integrated into the photonic integrated circuit built on a hybrid silicon platform. The device was composed 2 tunable lasers, 34 amplifiers, 32 photodiode and 32 phase shifters among other components (figure 2.7 below). The basic principle behind steering the beam in 2-D was wavelength tuning combined with optical phased array, because using optical phased array for 2-D beam steering required N^2 components compared to N components needed for 1-D beam steering. Utilising wavelength tuning reduced the number of components to N + M where M is the number of components in the tunable lasers [2]. The steering range achieved using this method was 23° x 3.6° with beam divergence of 1°.

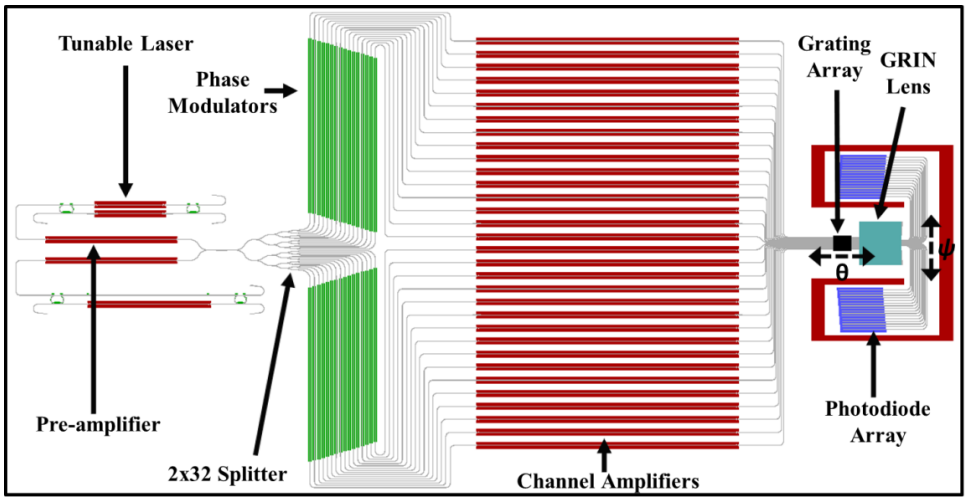

Figure 2.7 Fully integrated hybrid silicon 2-D beam scanner with 164 optical elements [2]

The table below summarizes the results from each of the optical phased array architectures described so far. Although high scan angles and low beam divergence can be achieved from these

OPA devices, the presence of secondary power in the side and grating lobes reduces their efficiency and accuracy of the scan.

	Largest scan angle achieved in any direction	Beam divergence
[10]	51°	3.3°
[16]	46°	0.85°
[29]	80°	0.14°
[2]	23°	1°

Table 2.1 Comparison of different OPA technologies in terms of scan angle and beam divergence

2.1.2 MICRO-ELECTROMECHANICAL SYSTEMS (MEMS)

Micro-electromechanical systems (or MEMS for short) has recently gained much popularity in beam steering applications. Many newly found companies specializing in LIDAR like Infineon [42] are now focusing on using MEMS technology in their LIDAR devices. A MEMS device consists of an IC chip with several microscopic components are integrated to make one complete mechanical system in microscopic form. It consists of micro-sensors, microelectronics and micromechanical systems. These devices work together to detect input signals and process the input to perform the corresponding mechanical output. MEMS components are all manufactured at the microscopic level, even components like levers, gears and motors are created in microscopic sizes. [31]

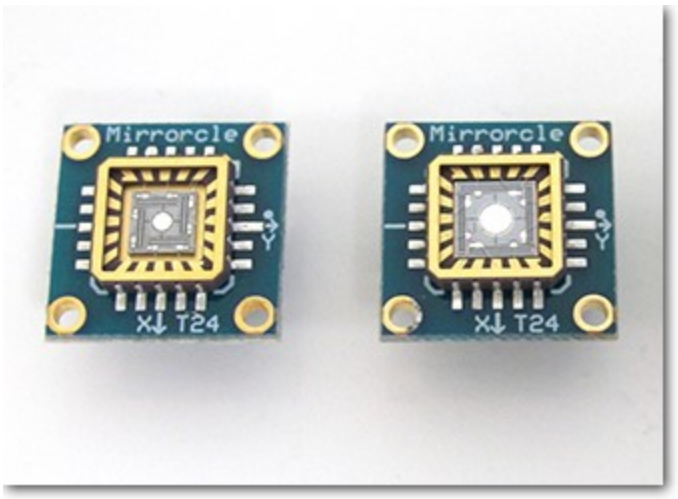

Figure 2.8 A MEMS scanning mirror [41]

MEMS based scanning mirrors are commonly used for LIDAR applications. These devices are composed of a tiny scanning mirror which is controlled by microelectronic and micro-mechanical elements which controls its direction of movement. An array of such MEMS based scanning mirror is what makes up a Digital Micro-mirror device, which is the main mechanism behind the beam steering system in [3] proposed by Smith et al. Each MEMS mirror in a DMD acts as a pixel which is all controlled by microelectronics that come together in the chip. The DMD is used in [3] to create a programmable blazed grating by controlling the individual mirrors using an Arduino controller. Discrete beam steering was demonstrated for five different angles corresponding to five different diffractions orders of the grating.

A collimated 8ns pulsed laser source was used with a wavelength of 905 nm. The beam scan at the five diffractions orders can be seen in figure 2.10 below.

It can be seen from the scan that there is presence of crosstalk between all the diffraction orders and the 0^{th} diffraction order. This crosstalk originates from the reflection at the mirror which causes detection from the 0^{th} order when the object comes close to the device. The device achieved scan angle of 48° and a measurement accuracy of less that 1cm.

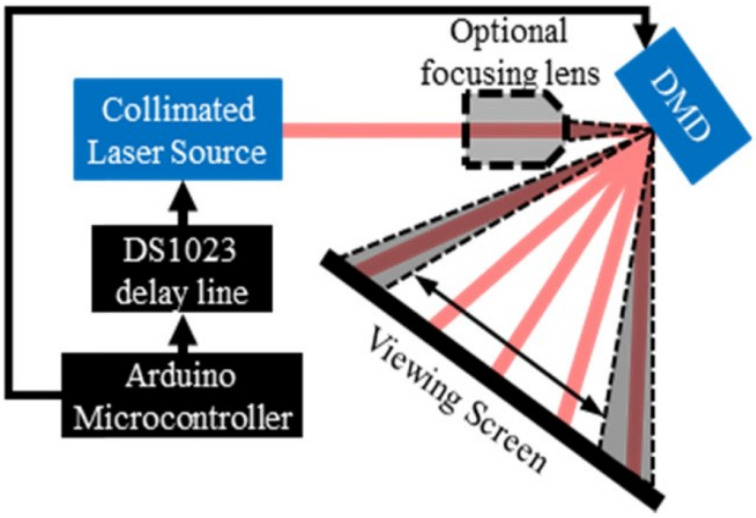

Figure 2.9 Setup of the beam scanning system using DMD [3]

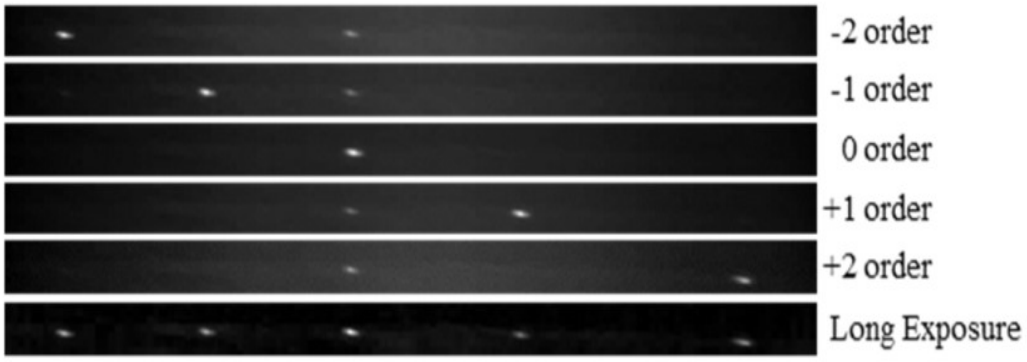

Figure 2.10 Beam scan using DMD showing the beam at 5 discrete beam scanning points. The presence of crosstalk between the other orders and the 0^{th} order can be seen in the scans. [3]

Hofmann et al. [45] introduced an automotive LIDAR device utilizing a MEMS scanning mirror coupled with an omnidirectional lens, which is capable of scanning in all directions. The device setup shown in figure 2.11 below consists of a 2-D MEMS scanning mirror capable of tilting by 15° on both axes. A large mirror aperture of 7mm diameter is selected to allow the device to measure larger distances. To facilitate circular scanning in all directions, a special tripod MEMS mirror was designed and fabricated.

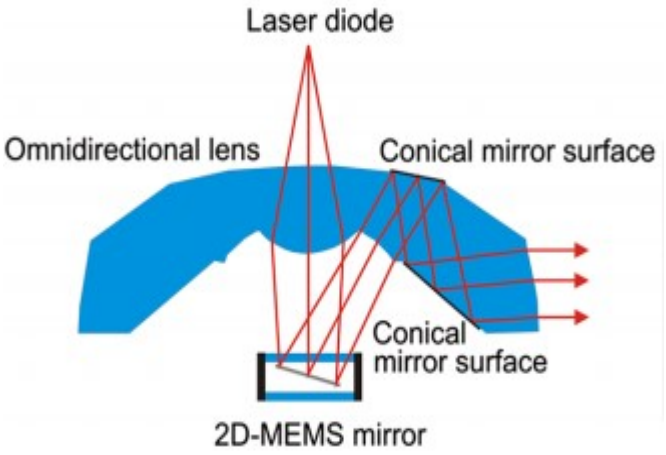

Figure 2.11 2-D MEMS scanning mirror coupled with omnidirectional lens [45]

2.1.3 BEAM STEERING WITH FOCUS TUNABLE LENSES

Wide-angle beam steering using focus tunable lenses was introduced by Zohrabi et al in [5]. Focus tunable lenses are composed of optical fluid enclosed in an elastic container which can change shape when pressure is applied to it in the form of electrical signals. The change in shape corresponds to change in the focal length of the lens. More details about focus tunable lenses are presented in the next chapter.

Zohrabi et al used two tunable lenses with other optical components to create a wide angle beam steering mechanism which is based on controlling the focal length of the two tunable lenses. Beam steering in 1-D was achieved with a total scan angle of about 78°.

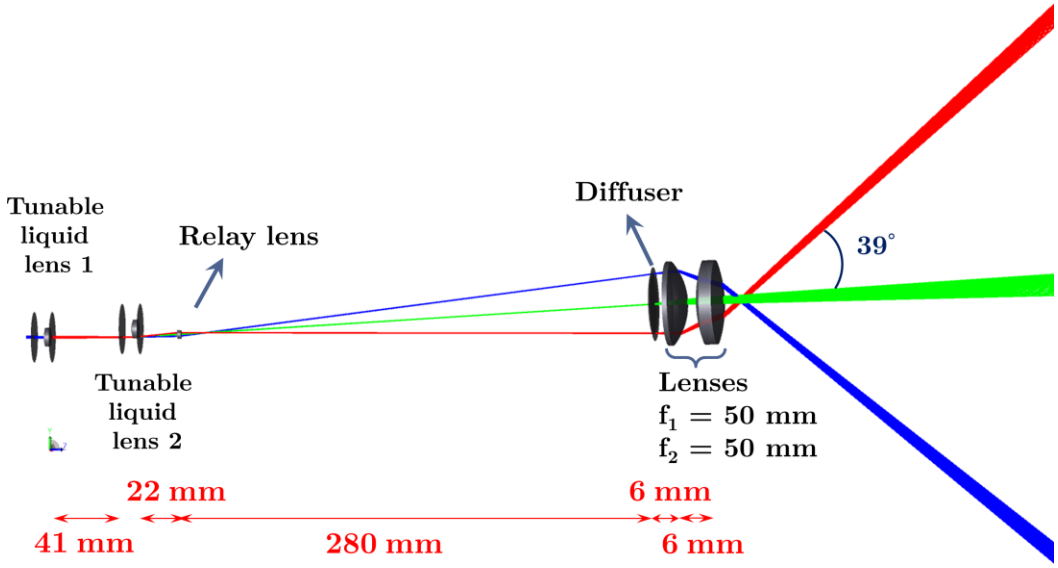

Figure 2.12 Beam steering using focus tunable lenses [5]

The major drawback here however is the large size caused by the length of the optical path. The device was modified to scan in 2-D by adding a third tunable lens, and the scan range was increased to ±75° by employing a fisheye lens to widen the scan. This however further increases the device size. The figure 2.13 below shows the position of the third tunable lens for 2-D scanning with the fisheye lens to widen the scan angle further. It can be seen that the fisheye lens contributes to increasing the size of the device further. Figure 2.14 shows the scan results from both setups. The first figure 2.14 (a) shows a 1-D scan of 39° on either side from the center resulting in a total scan angle range of 78° whereas (b) shows the beam travelling 75° on either side resulting in a 150° scan.

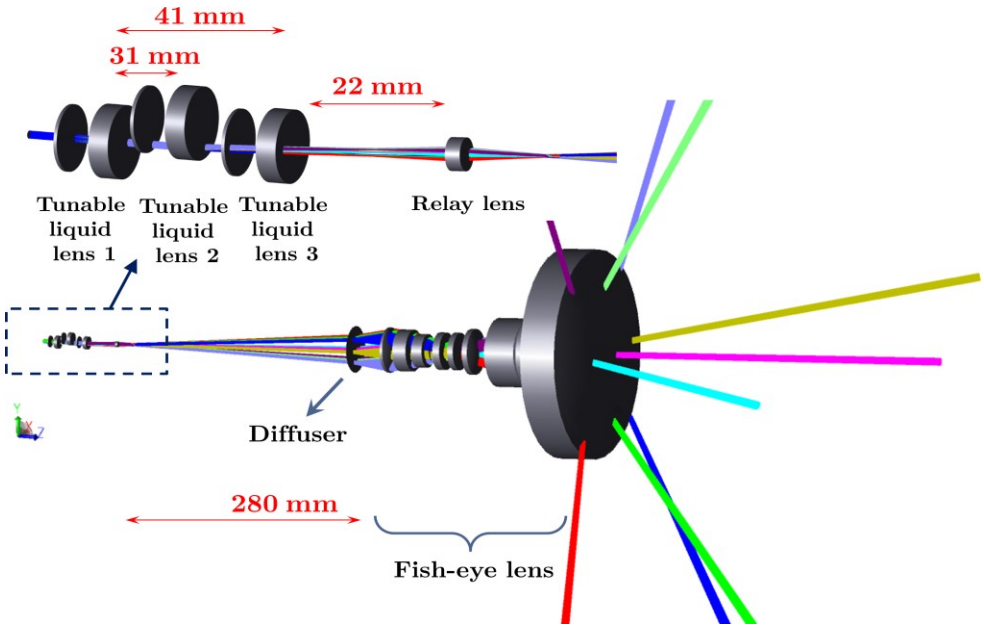

Figure 2.13 Increasing scan angle using fisheye lens [5]

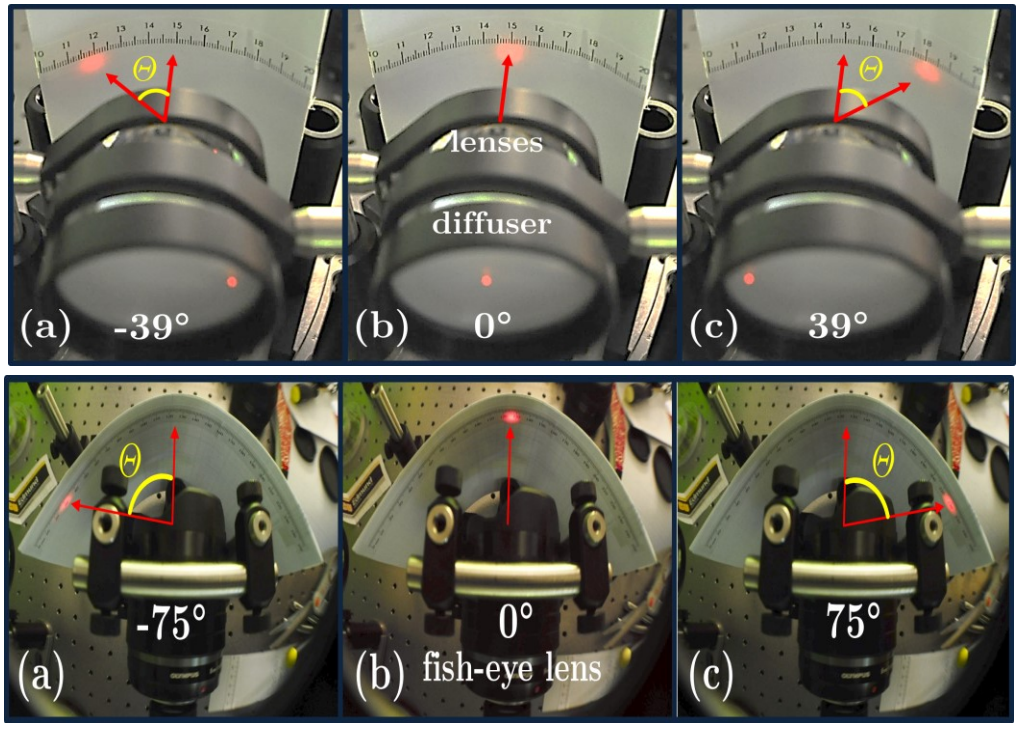

Figure 2.14 Experimental setup of the device (a) without and (b) with the fisheye lens showing scans of ±39° and ±75° respectively [5]

3. BEAM STEERING USING FOCUS TUNABLE LENSES

3.1 FOCUS TUNABLE LENSES

The key mechanism used in controlling the direction of the laser beam in this work is focus tunable lenses developed by Optotune. The basic structure of the focus tunable lens comprises of optical fluid (with low dispersion, and refractive index of 1.30) enclosed in an elastic container with sealed ends. The tunable lens is driven by electric current which controls the pressure exerted on the elastic container housing the optical fluid thereby changing the shape of the container. This change in shape corresponds to the change in the radius of curvature of the lens, and therefore the focal length is controlled through the input current. The optical power of the lens (which is the inverse of the focal length), varies linearly with the current. [11]

Figure 3.1 Optotune's EL-10-30-TC focus tunable lens [13]

The range of values between which the focal length of the lens can be tuned depends on the membrane thickness of the container enclosing the optical fluid. Larger ranges of focal length can be achieved from lenses made of thinner membranes than those with thicker ones. Most lenses

have optical powers which can only be tuned between positive values i.e. they can only act as convex lenses. Other lens models have a concave offset lens to provide negative optical power values. Some models also have the capability to use the pressure exerted on the lens membrane to create a concave lens shape. [11]

Another important parameter of consideration when using focus tunable lenses is the response time. Due to the inertia of the optical fluid, there is a slight delay in the application of current to the change in the focal length of the lens. The response time is usually a few milliseconds and can vary between 2-12 milliseconds depending on the model of the lens. [11]

3.1.1 ELECTRICALLY TUNABLE LENS EL-10-30

The EL-10-30 is the most versatile plano-convex lens model made by Optotune. Although the optical power can only take positive values, it has one of the largest range of values for tuning the focal length. And it is also capable of reaching the greatest optical power (up to 20 diopters) compared to all the other lens models. The EL-10-30 comes in two different types of housing, the EL-10-30 TC which is a compact version, and the EL 10-30-C. The two models have similar specifications except for some differences in dimension and focal tuning range which is summarized in Table 3.1 below. [12]

Lens model	Dimension (mm)	Focal length tuning range	Optical power range (diopter)
EL 10-30 TC	30 x 10.7	+50 to +120	+8.3 to 20
EL 10-30 C	30 x 20	+100 to +200	+5 to +10

Table 3.1 Comparison of two different tunable lens models

The graph below shows the relationship between optical power and current for the different EL-10-30 lens models. The two variations of the C model differ only in that the second model comes with an option for an offset lens which allows for the lens to reach negative optical powers. The optical power can then be tuned from -1.5 to 3.5 diopters, and so the range remains the same. [12]

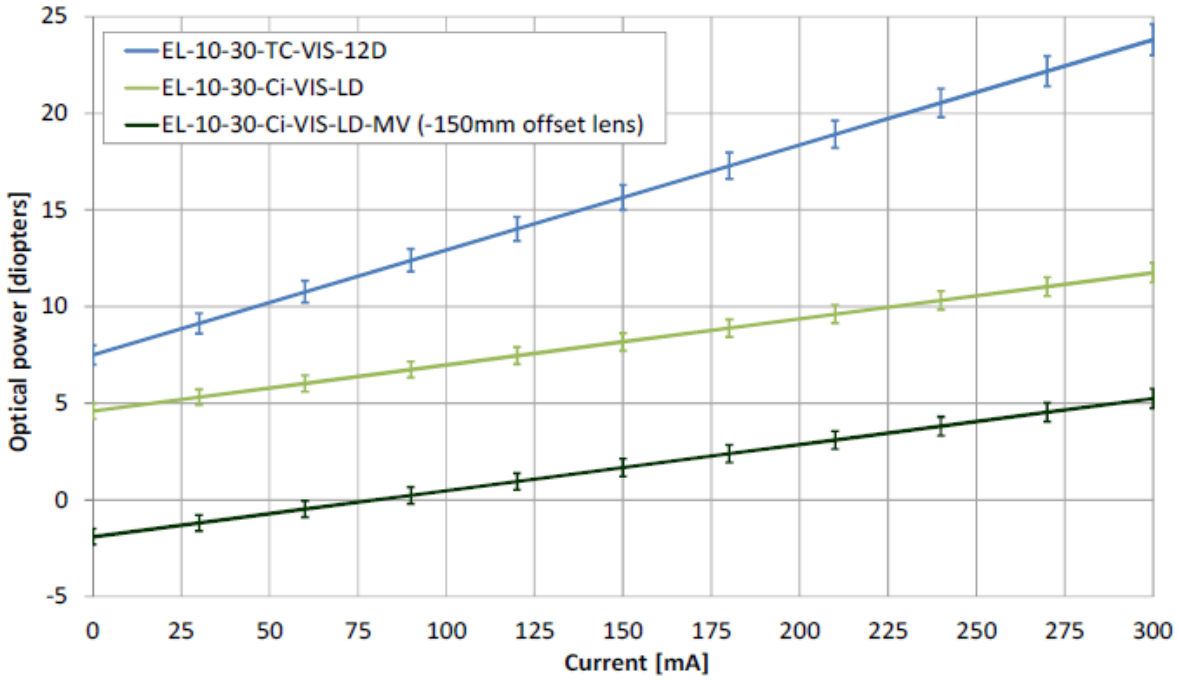

Figure 3.2 Optical power vs current for the EL-10-30 series [12]

Nominal values of input current for the lens are between 0-250 mA, although currents up to 400 mA can also be applied. [12] It can also be seen from the slope of the different lines, that the EL-10-30 TC has a greater range of optical power values for the same input current.

For this work the EL 10-30 TC model was chosen because of two reasons. First, the EL 10-30-TC is smaller in size compared to the EL 10-30 C model, which is important for making our design as compact as possible. Secondly, the TC model also has a thinner membrane which is why it is capable of achieving higher optical power and has a greater range of optical power tuning which

is also essential for a more compact device, as it can produce a larger scan within a shorter optical path length. The EL 10-30 model also has the smallest response time of less than 2.5 milliseconds among all the tunable lens models. [12]

3.2 ZEMAX DESIGN SOFTWARE

Zemax OpticStudio software was used for simulating the beam scanning system. OpticStudio is a powerful tool for designing all kinds of optical systems and analyzing them using its ray tracing feature. It has two modes of operation: sequential and non-sequential mode.

3.2.1 SEQUENTIAL MODE AND NON-SEQUENTIAL MODE

Sequential and non-sequential design modes differ mainly in the way the light rays propagate through the system. In sequential design, rays follow a predetermined path hitting each object in the exact sequence as they are defined in the Lens Data Editor. Analysis of stray light or light scattering is impossible in the sequential mode as the light rays (which are predefined by the editor) cannot follow random paths in a system. For such analyses, the non-sequential mode is useful. In the non-sequential mode, rays defined in the design do not follow any predefined sequence. The path followed by the ray and the sequence of objects the ray hits completely depends on the direction of the ray and the position of the object. [17]

The two modes also differ in the way objects are defined. In the sequential mode, each object is defined by its individual surfaces. For example, to create a plano-convex lens, two individual surfaces must be created: the lens front which will define the radius of curvature of the lens, and a flat lens back which will have a radius of curvature of zero. On the other hand, in the non-sequential

mode, objects are defined as a whole and not as individual surfaces. Therefore, the same plano-convex lens can be defined as one object. [17]

The non-sequential mode is a more versatile tool as any kind of 3-D surface can be modelled in it. Non-sequential mode was utilized in this work, as the design involved the use of many objects that can only be modelled as non-sequential objects in Zemax like prisms and a diffuser. [17]

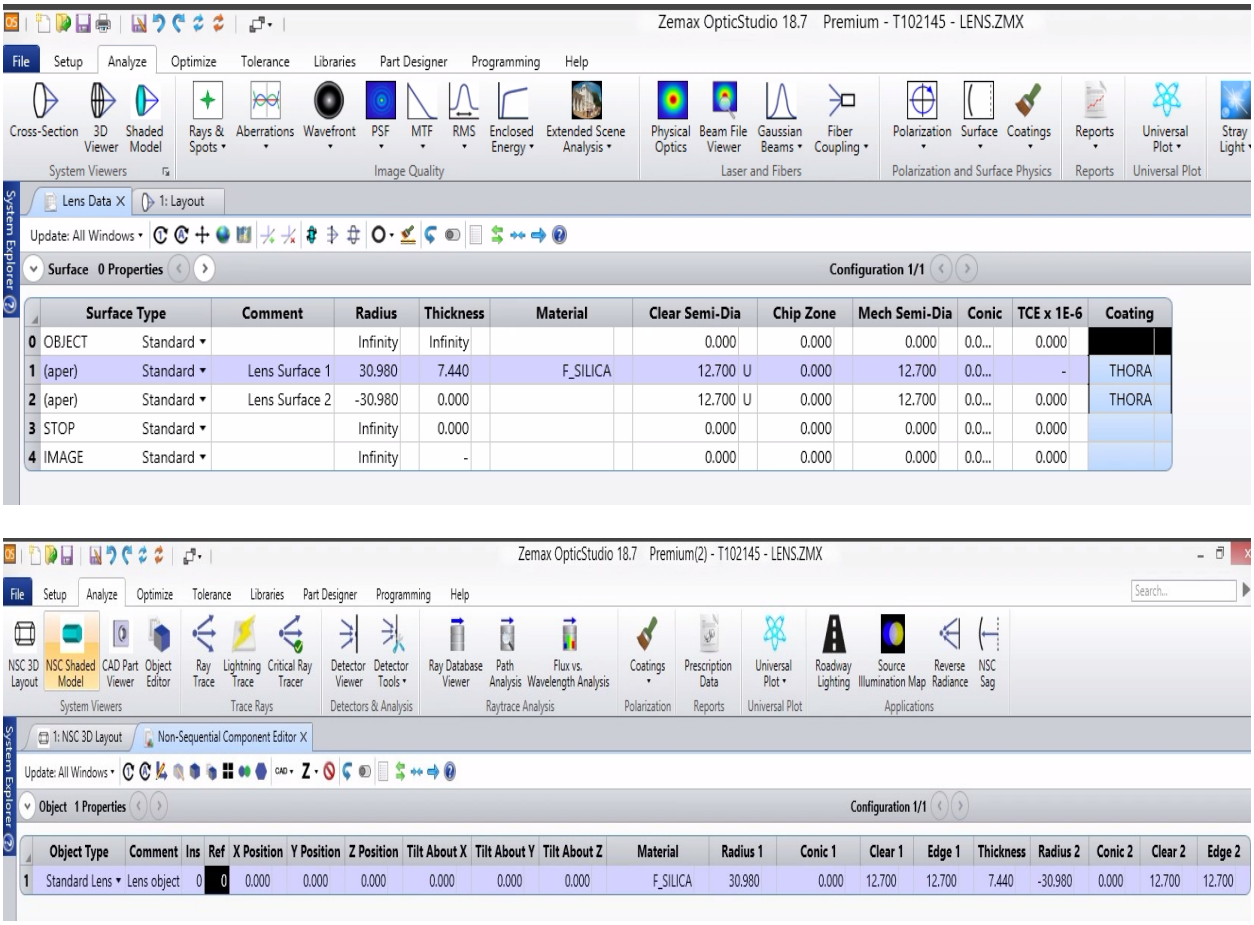

Figure 3.3 Modelling a simple lens using Sequential and Non-Sequential mode in Zemax OpticStudio. The lens is modeled as two separate surfaces in the Sequential mode whereas it is modeled as a single object in the Non-Sequential mode

3.3 SYSTEM ELEMENTS AND DESIGN

3.3.1 MODELLING TUNABLE LENSES IN ZEMAX

The Zemax model for the EL-10-30 TC and other tunable lens models can be found from the Optotune website [12]. The Zemax model for the EL-10-30 TC is shown in figure 3.4 below. The focal length of the lens can be tuned between +50 mm to +120 mm, although only the radius of curvature can be modified in Zemax. Using Zemax simulation and measurement, the radius of curvature of the lens was found to be 14mm when the focal length was set to 50 mm. In the same way, the radius of curvature corresponding to a focal length of 120 mm was found to be 38mm. Therefore, the radius of curvature of the lens is tunable between 14mm to 38mm.

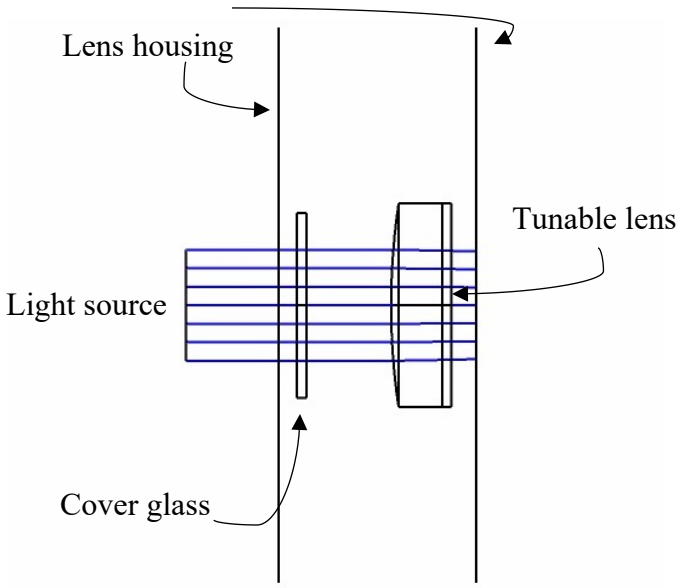

Figure 3.4 Zemax model for EL 10-30 TC modeled in Sequential mode of Zemax. The complete model shows the tunable lens along with the lens housing and cover glass

Figure 3.5 below demonstrates the focal point of the lens when the radius of curvature is set to 14 mm and 38 mm respectively.

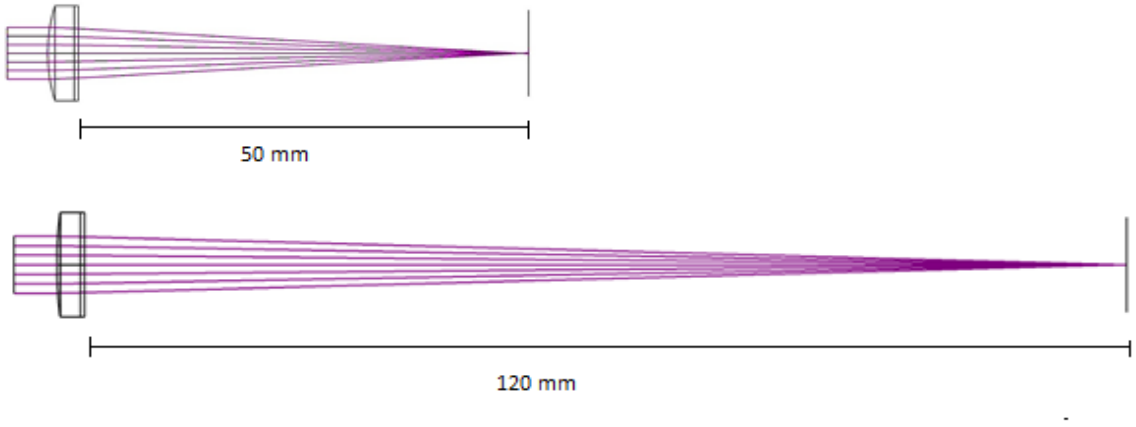

Figure 3.5 Tunable lens focal length set to 50 mm and 120 mm

3.3.1.1 EFFECT OF CHANGING CURVATURE OF ONE LENS ON THE BEAM

To demonstrate the effect that changing the focal length on the optical beam, the beam must be decentered along the y axis with respect to the lens. In figure 3.6 below, the beam is decentered by 2 mm on the y axis, and the focal length is set to 20mm by setting the radius of curvature of the lens to 6mm (this is beyond the range of the actual lens, but it is used for the sole purpose of demonstration). With the object at the same distance from the lens, the radius is now changed to 5mm and then 7mm. It can be seen from the figures, that the beam changes position on the object, but it becomes defocused on the object. Therefore, to move the beam and still keep it focused at the same distance from the lens, two tunable lenses must be used, as discussed in the next section. [5]

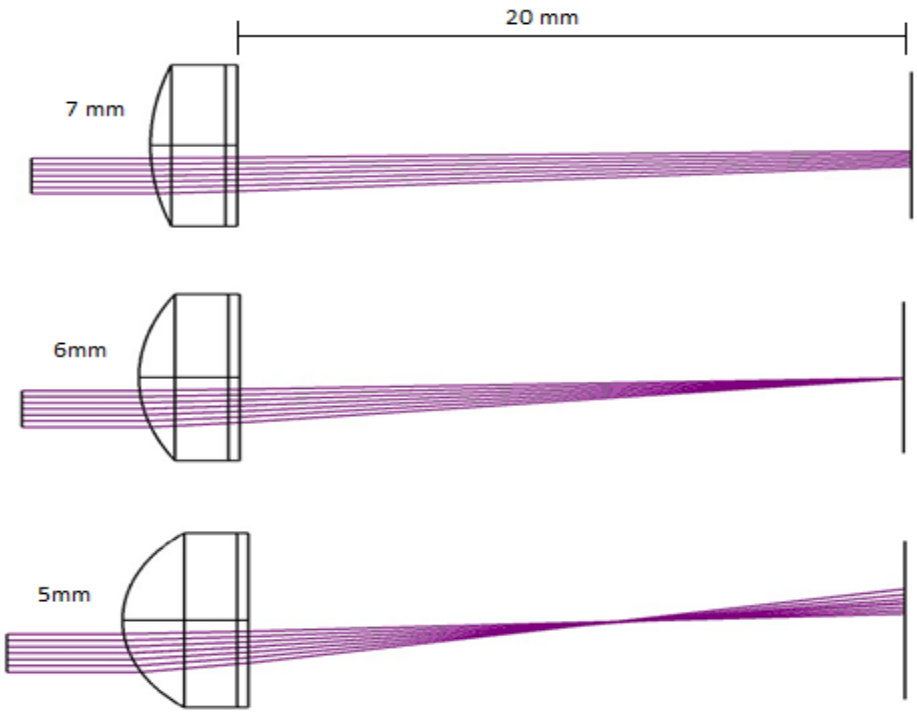

Figure 3.6 Effect of adjusting the radius of curvature of the lens on the beam. The radius of curvature is set to 5, 6 and 7 mm.

3.3.1.2 STEERING A BEAM WITH TWO TUNABLE LENSES

To steer the beam and also keep it in focus on the image plane, two lenses must be used. In figure 3.7 below, the two lenses are placed 15mm from one another, and the second lens is decentered 4.3mm along the y axis with respect to the first lens. The radius of curvature of both lenses is set to 25mm and the beam focuses 45 mm away.

In the second image the radius of curvature of the two lenses are now changed to 19 and 37 mm respectively. The beam focus displaces by 0.7 mm on the y axis, indicating beam steering on the y-axis. However, the beam still remains focused at the same distance of 45 mm.

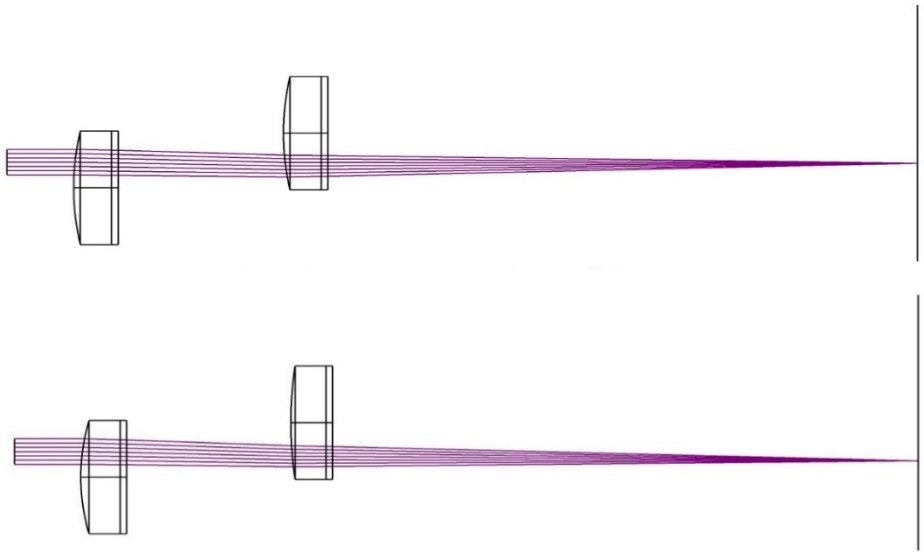

Figure 3.7 Beam steering using two tunable lenses

3.3.2 RELAY LENS

An achromatic doublet lens is placed after the second tunable lens and it acts as a relay lens to focus the beam from the tunable lenses. The architecture of an achromatic doublet lens consists of two lenses attached together one with a positive focal length and the other with a negative focal length. The two lenses are also made with materials of different indices of refraction, and different dispersion characteristics. Achromatic doublet lenses are commonly used to correct the effects of chromatic and spherical aberrations. [18] The lens model used here is equivalent to the model AC080-010-C-ML from Thorlabs, with a focal length of 10mm [23]. The lens works to focus the incoming laser beam from the tunable lenses onto the diffuser [5]. The diagram below shows the achromatic doublet lens modeled in Zemax.

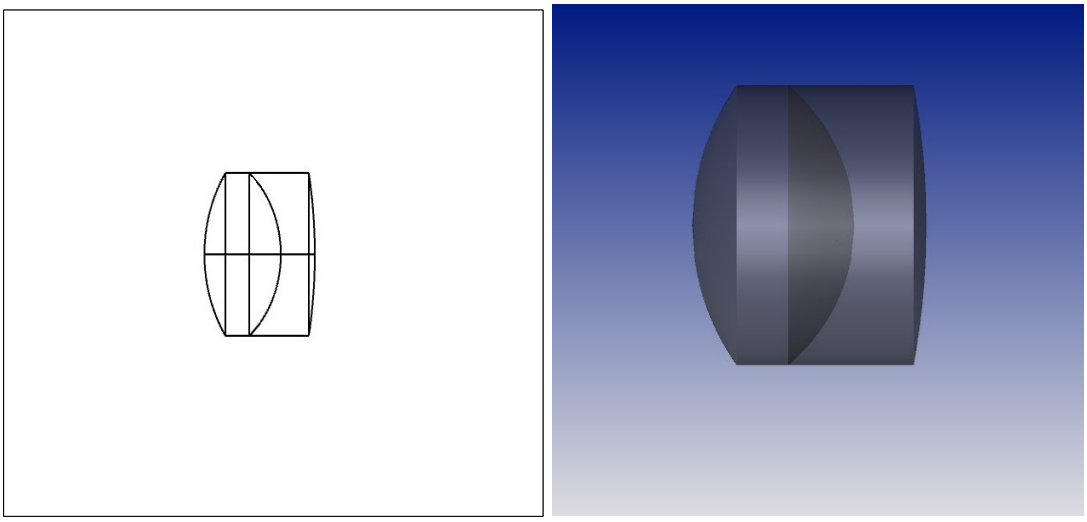

Figure 3.8 Model of the achromatic doublet lens on Zemax

3.3.3 FOLDED OPTICS

The optical path length between the achromatic doublet lens and the diffuser in [5] plays an important role in determining the scanning angle range of the design. Because of the high focal length of the tunable lenses, to achieve significant steering of the optical beam, a very high path length is required between the relay lens and the diffuser. And this high optical path length makes the design very large, making it impractical.

To tackle this issue, the principle of folded optics was used. The idea here is to fold the optical path thereby reducing its longitudinal size. A similar idea is used in binoculars that use Porro prism. Two prisms are set with their bases facing each other with one prism rotated along one axis with respect to the other. This reduces the size of the binoculars by reducing the optical path length. [20]

The setup used in this work is shown in figure 3.9 below, with two 90° prisms with their base facing each other. When the light enters the through the base of the first prism, total internal

reflection occurs when it hits the other two faces of the prism. The light then exits the first prism in the opposite direction and enters the second prism through its base and repeats the process.

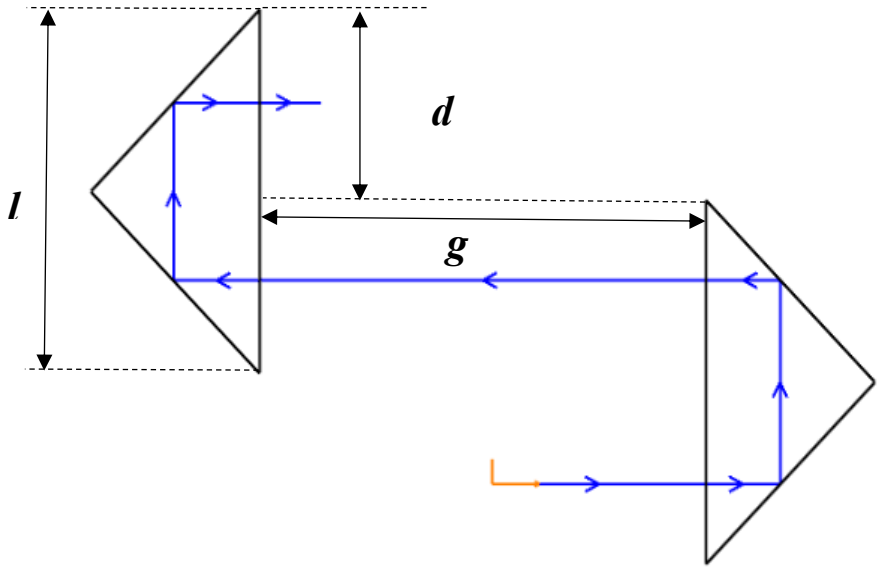

Figure 3.9 Prism layout for folding the optical path

For the above process to take place, the prism base length *l,* the distance between the prisms *g,* and the displacement along the base *d* must be selected to that the light rays enter both the prisms and total internal reflection takes place in both prisms. In general, for the arrangement shown in figure 3.9 above, incoming beam will go through 2N total internal reflections, and N is determined by the formula:

$$N = round\left(\frac{l}{d}\right) \qquad (3.1)$$

Where *round* refers to rounding the result to the nearest integer. If *g* is the length of the gap between the prisms, and n is the refractive index of the prism material, the total optical path length that the beam will now travel is given by the formula [19]:

$$\Delta = nNl + Ng \qquad (3.2)$$

The dimensions used in this work are shown in figure 3.10 below. The prisms used had a base length of 28 mm and were placed 40 mm apart, and displaced by 14 mm. The material used was N-BK7 glass with a refractive index of 1.5 at 1550 nm wavelength. Using equation 3.1 above, with these values gives us N = 2, and as seen from the figure below, the beam experiences total internal reflection 4 times.

Using these values in equation 3.2 above, we get the total optical path length as

$$\Delta = 164\ mm$$

Indicating that the beam travels a total of 164 mm between the two prisms.

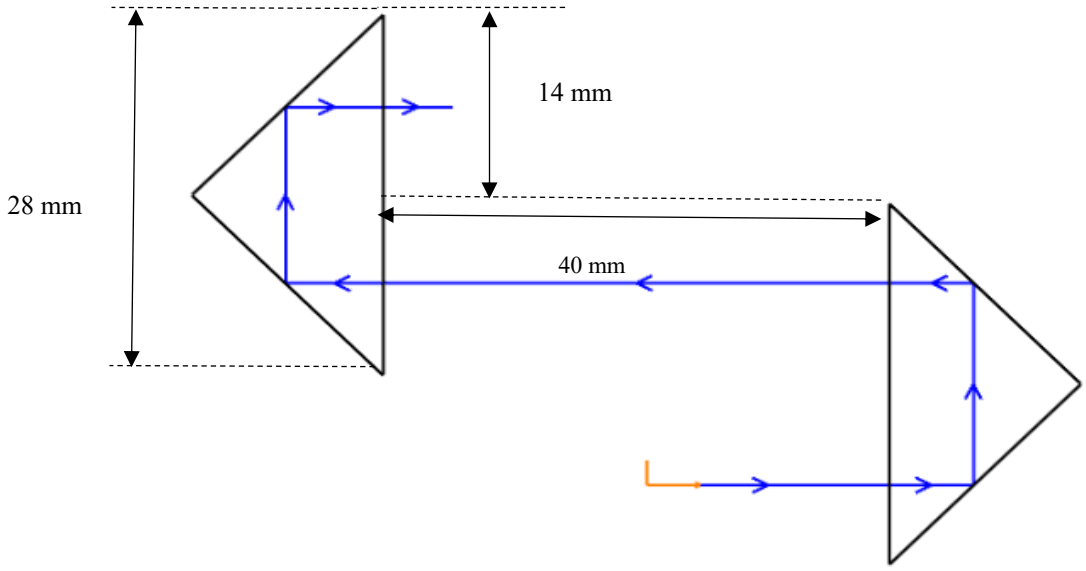

Figure 3.10 Dimensions used for prism layout

3.3.4 OPTICAL DIFFUSER

Optical diffusers are used to scatter or “soften” the light passing through them. They are made of different materials, and the most common diffusers are made with N-BK7 ground glass material. [21] The light is focused onto the diffuser from the relay lens and it acts as a point source of light whose position depends on the focal length of the tunable lenses. The diffuser increases the numerical aperture of the beam so that the beam can be steered through a larger angle.

The diffuser is modelled in Zemax as a cylindrical volume object. The back face of the cylindrical object has a BSDF scatter model with a scatter angle of 15°. This emulates the working principle of a ground glass N-BK7 diffuser with a diffusion cone angle of 15°. The diagram below shows the effect of the diffuser on the incoming laser beam.

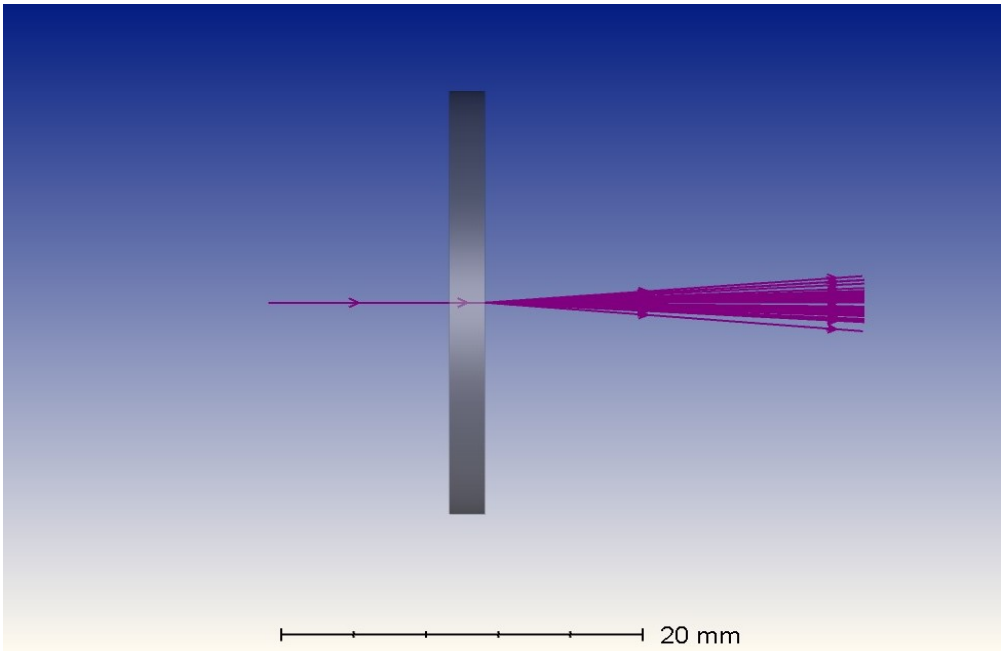

Figure 3.11 Diffuser modeled in Zemax OpticStudio with a diffusion cone angle of 15°

3.3.5 OBJECTIVE LENSES

The final step in the beam steering process is further increasing the scan and focusing the beam using two objective lenses. The objective lenses also collimate the diverging beam coming from the diffuser which acts as point source. A plano-convex and a double convex lens is used one after the other to focus the beam emitted from the diffuser onto the detector. The lenses used in the final design are equivalent to models LA 1951.1 and LB 1761.1 by Thorlabs both with focal lengths of 25 mm. [23] Objective lenses with a focal length of 50 mm were used in [5], but a lower focal length was used in this work as it leads to a higher range of scanning angle. The lower focal length also works to reduce the divergence of the beam and create a more collimated beam as will be seen later.

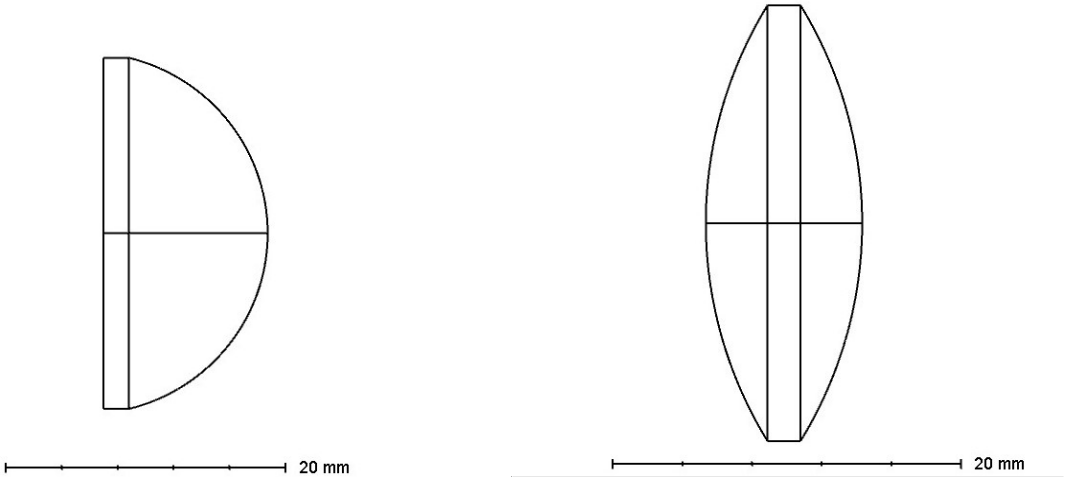

Figure 3.12 Plano-convex and double convex objective lens models on Zemax with focal lengths of 25mm

3.4 SIMULATION AND RESULTS

This section discusses the simulation results for the different versions of the design. Three different simulations were made which will be discussed. The first one replicates the design and result of that obtained by Zohrabi et al in [5]. Since the design is far too large in size because of the optical path length between the relay lens and the diffuser, the effect of reducing the optical path length is also discussed. Finally, folded optics is incorporated in the design along with objective lenses with a smaller focal length. Folded optics reduced the longitudinal size of the device, whereas the change in focal length of the objective lenses increased the scan angle and resulted in a more collimated beam.

3.4.1 CASE 1

In the first simulation, the tunable lenses were placed 41 mm away from one another and the relay lens was placed 22 mm away from the second tunable lens. The diffuser was placed 280 mm from the relay lens, and objective lenses 50 mm in focal length followed the diffuser placed 12mm and 6mm apart. The rays start from the source object to the left of the first tunable lens and are finally cast onto a detector that is placed 85 mm from the last lens surface. Three beams are displayed in the figures below, slightly displaced along the lens on the y-axis. This replicates the effect of changing the radius of curvature of the tunable lenses while keeping the source in the same position. The detector here acts as the object which will be scanned by the LIDAR system. The detector comes with ray tracing capabilities, with which we can detect the position of the ray on it for a specific focal length of the tunable lenses. The ray trace shown in figure 3.15 shows the position of the ray on the detector when the radius of curvature of the lens is adjusted to different values.

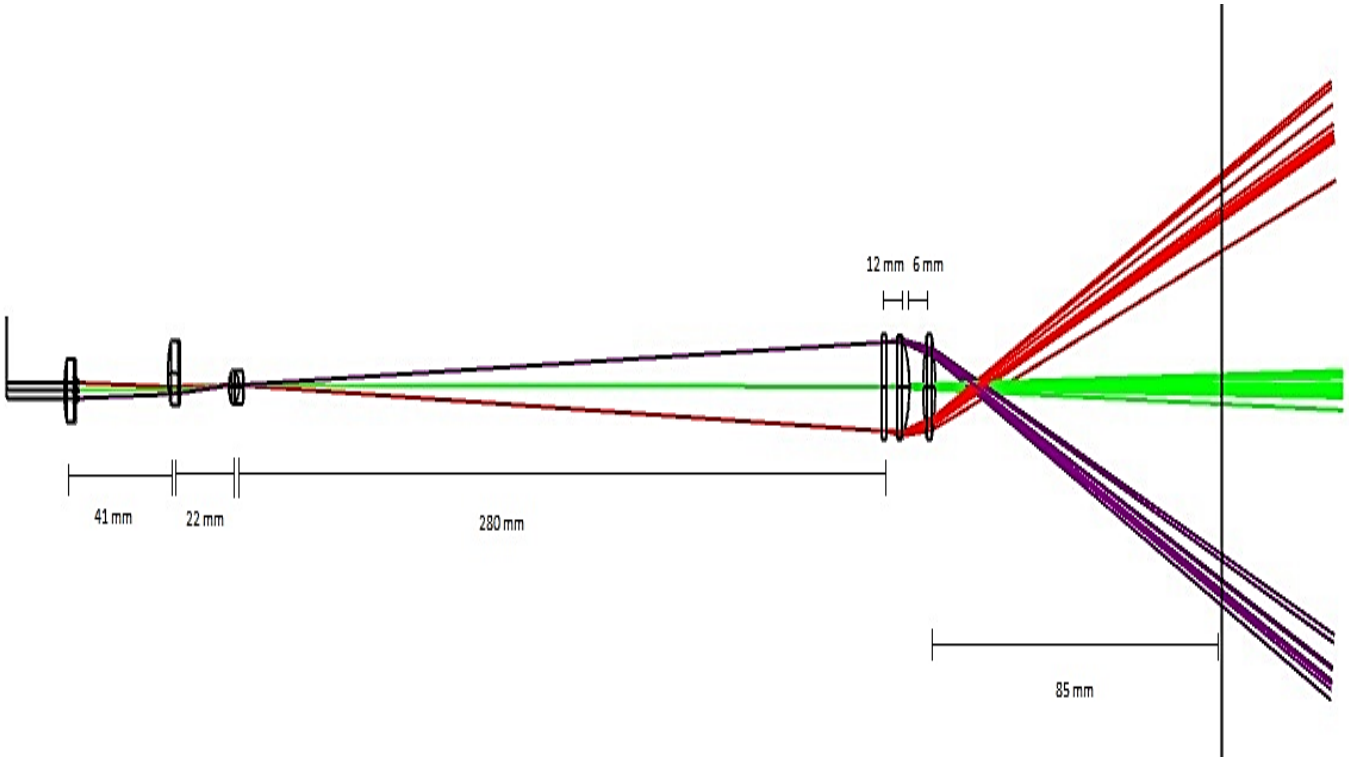

Figure 3.13 3-D cross section model for Case 1

From the 3-D model shown above, it can be seen that there is a big gap between the relay lens and the optical diffuser. This gap is necessary to provide sufficient path for the light rays to travel and fall on the right point on the diffuseraf to ensure wide angle scanning. The entire device setup is 385 mm long which is a drawback as the device too large for practical use in LIDAR systems.

The scan angle is calculated from the ray trace results shown below. The diagrams show the results obtained from the ray tracing tool in Zemax. Figure 3.15 (a) shows the physical position of the beam falling on the detector when the radius of curvature of the tunable lenses are tuned between the values of 14 mm and 38 mm. It can be seen that the beam changes position along the y-axis demonstrating 1-D beam steering along the y-axis. The same result is represented in graphical form with the incoherent irradiance, which is a measure of the intensity of the beam, plotted against its position on the y-axis.

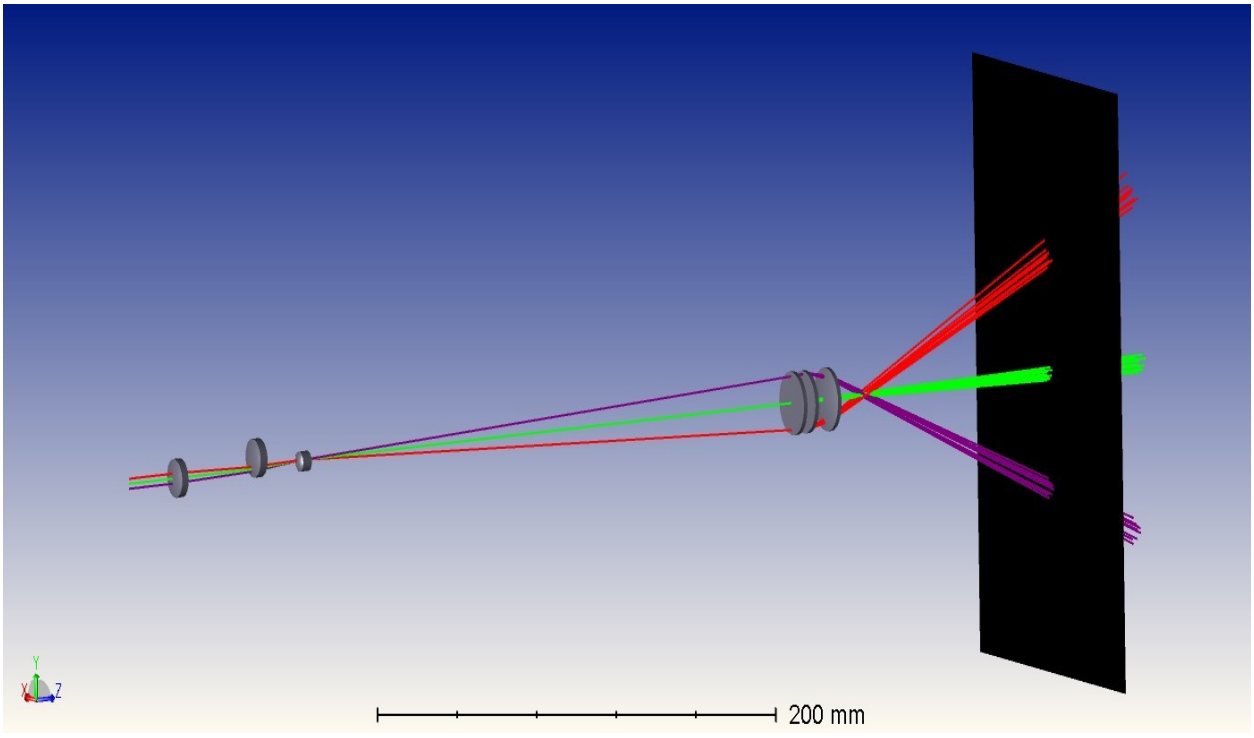

Figure 3.14 3-D shaded model for Case 1

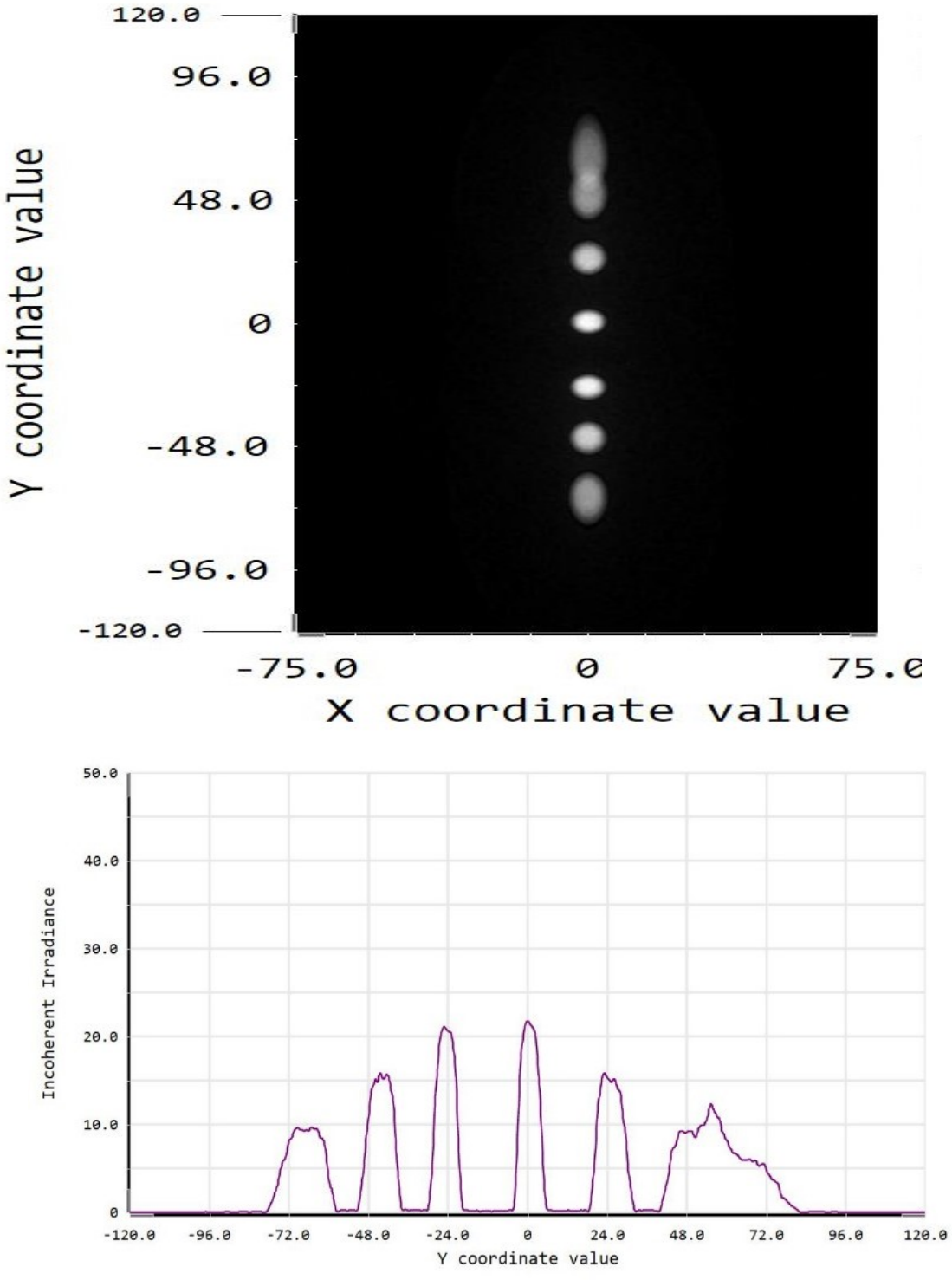

Figure 3.15 Diagram showing the results from the ray tracing tool in Zemax. (a) shows the physical position of the beam moving along the y-axis at different values of focal length of the lenses. The incoherent irradiance of the beam is the measure of the intensity of the beam. (b) shows the same result in graphical form making it easier to locate the beam on the y-axis

Figure 3.15 (b) shows the location of the beam's peak more accurately. It can also be observed that the beam instensity falls as it moves further away from the center where it is at its peak. This drop in intensity also coincides with the fact that the beam diverges more as it is steered further from the the center. This increase in beam size results in an overlap of the rays traced at y-coordinate positions +45 and +66 on the detector.

The beam from the device falls onto the detector which is placed 85mm away, and moves up to 66mm away from its center position on the y-axis. This is represented in figure 3.16 below.

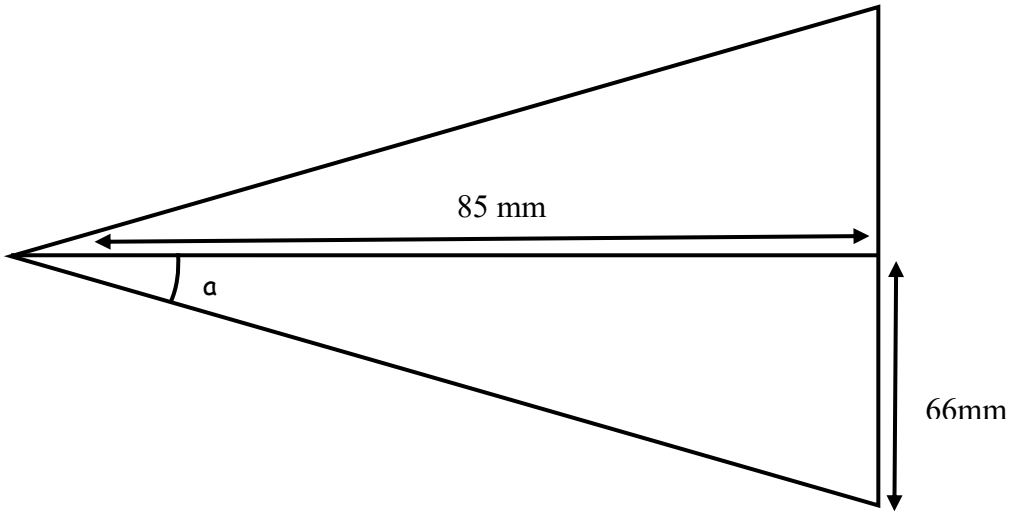

Figure 3.16 Calculating beam scan angle. The base of the triangle represents the detector on which the beam travels along the y-axis.

Using rules of trigonometry, as shown below, α is found to be 37.8° meaning the beam moves 37.8° on both sides away from the center. Therefore the total scan angle is found to be 76°.

$$\alpha = \tan^{-1}\frac{66}{85}$$

$$\alpha = 37.8°$$

$$\text{Total scan angle} = 2\alpha = 76°$$

Although this design is capable of scanning over a wide angle, the major drawback is that the long optical path makes the device very big. The effect of reducing the optical path will result in a much smaller scan angle as will be seen in the next section.

3.4.2 CASE 2: REDUCING THE OPTICAL PATH LENGTH

In an attempt to reduce the longitudinal size of the device, the optical path length between the relay lens and diffuser was reduced from 280mm to 55mm. The tunable lenses were placed 10mm apart and the relay lens was placed 12 mm from the second tunable lens. The resulting ray trace is shown below, with the detector placed at the same distance from the last surface (85 mm). It can be seen that there is a significant reduction in the scan angle once the optical paths are reduced.

From the ray trace results shown in figure 3.19, the beam moves 12 mm on the y axis in both directions away from its center position. Using the same principle as in section 3.4.1 above, the scan angle is calculated as 8° in both directions, resulting in a total scan angle of 16°.

In this version of the design, the size of the device is reduced to only 114 mm, but the corresponding steering range is too small. The next design attempts to tackle this by employing folded optics to tackle the issue of size and at the same time increase the scan angle to a higher value.

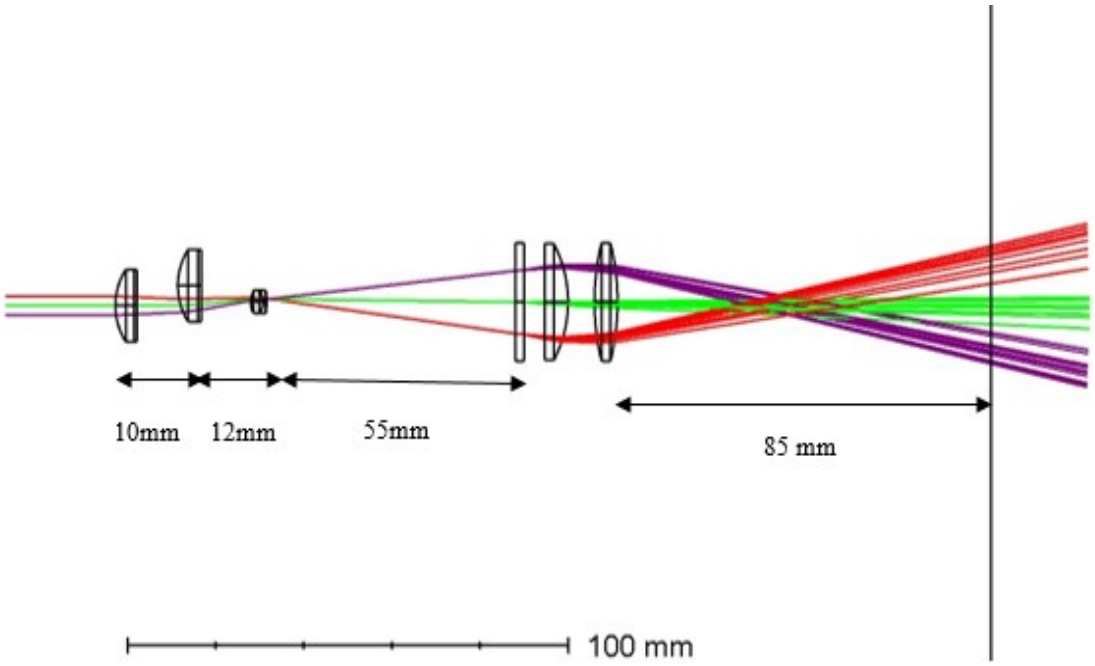

Figure 3.187 3-D cross section model for Case 2

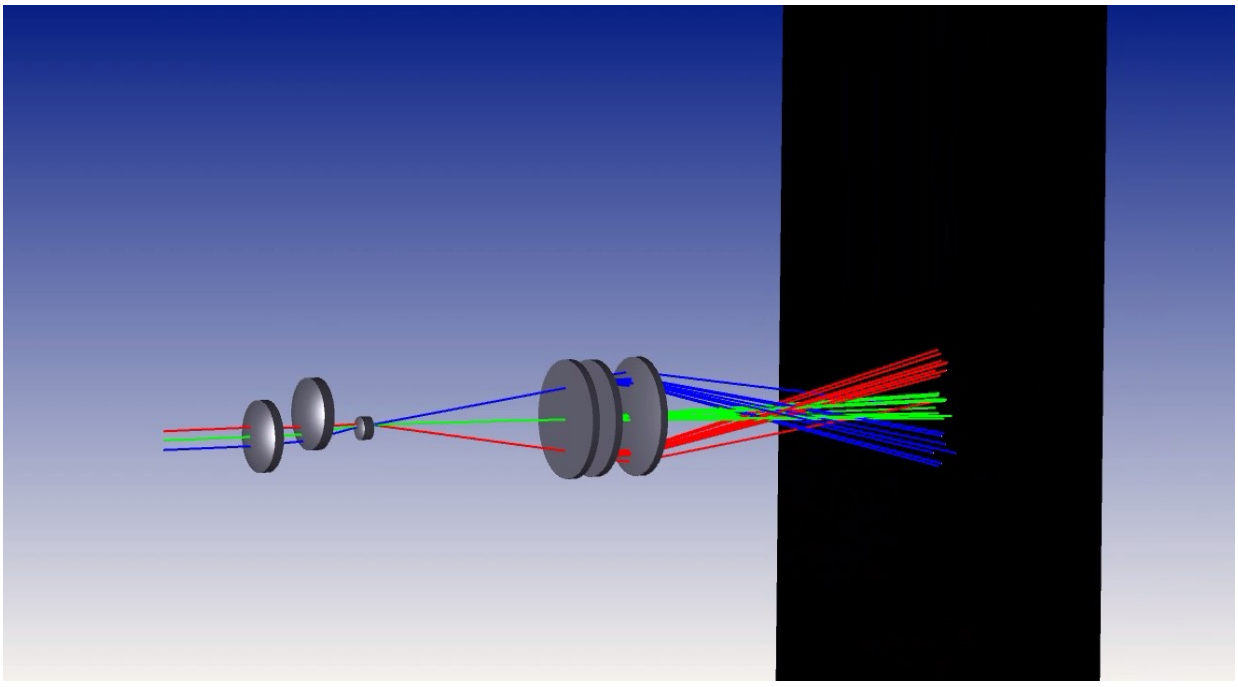

Figure 3.178 Shaded model for Case 2

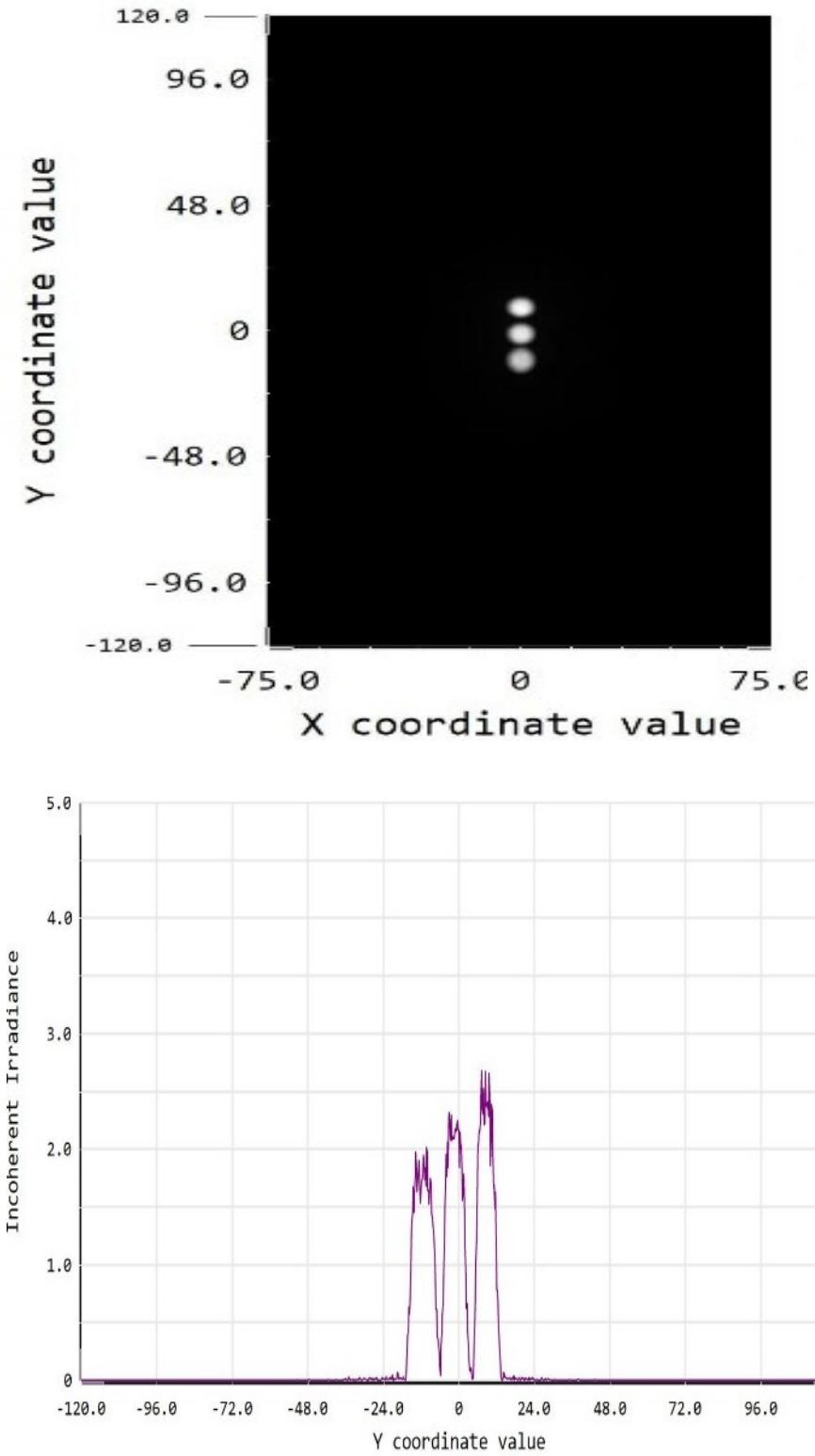

Figure 3.19 Ray traces obtained from the design after reducing the optical path length shows its effect. It can be seen that the beam moves between a much smaller range than before

3.4.3 CASE 3: INTEGRATING FOLDED OPTICS INTO THE DESIGN

In an effort to reduce the length of the device, and at the same time increase the scan angle, two design changes were made:

- Prisms were used in the optical path between the relay lens and the diffuser to fold the path of light, thereby reducing its length
- Objective lenses with lower focal lengths value were used after the diffuser to increase the scan angle.

In this final design, the tunable lenses are placed 10 mm apart and the relay lens is placed 15 mm from the second tunable lens. The 280 mm optical path between the relay lens and the diffuser in the first design, is replaced by the prism arrangement shown in figure 3.10 earlier. The diffuser is placed 60 mm after the base of the second prism with objective lenses of 25 mm focal length following the diffuser.

Figure 3.22 shows the results of the ray trace. It can be seen that the beam now travels between farther along the y-axis. From figure 3.22 (b) the beam is measured to steer 42 mm away from the center on both sides. Using the same calculations as 3.4.1 above, this corresponds to a steering of 26° on both sides, meaning a total scan angle of 52°. This is a significant increase in the scan angle from the last design. At the same time, it can be seen from the figure above that the entire length of the device is about only 119 mm which is also a major reduction in size from the first model.

Furthermore, it is visible from the two ray trace diagrams and the 3-D model that the higher power of the objective lenses are much more efficient in producing a low divergence beam with higher values of incoherent irradiance.

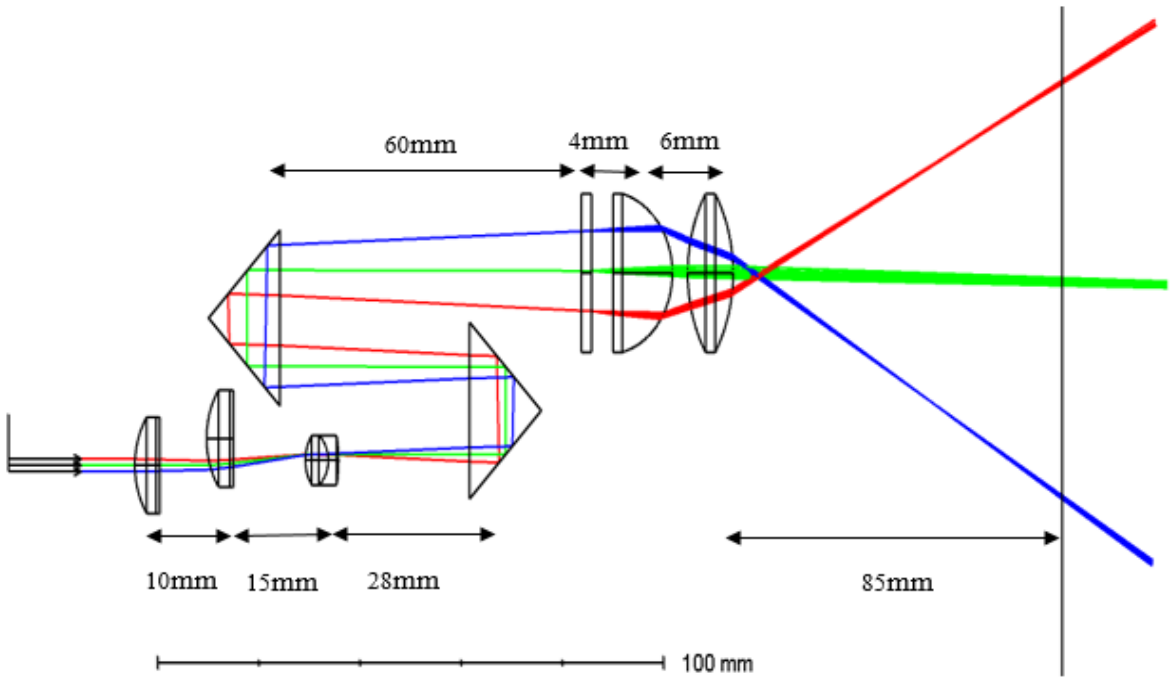

Figure 3.20 3-D cross section model of final design using prisms and objective lenses with a smaller focal length

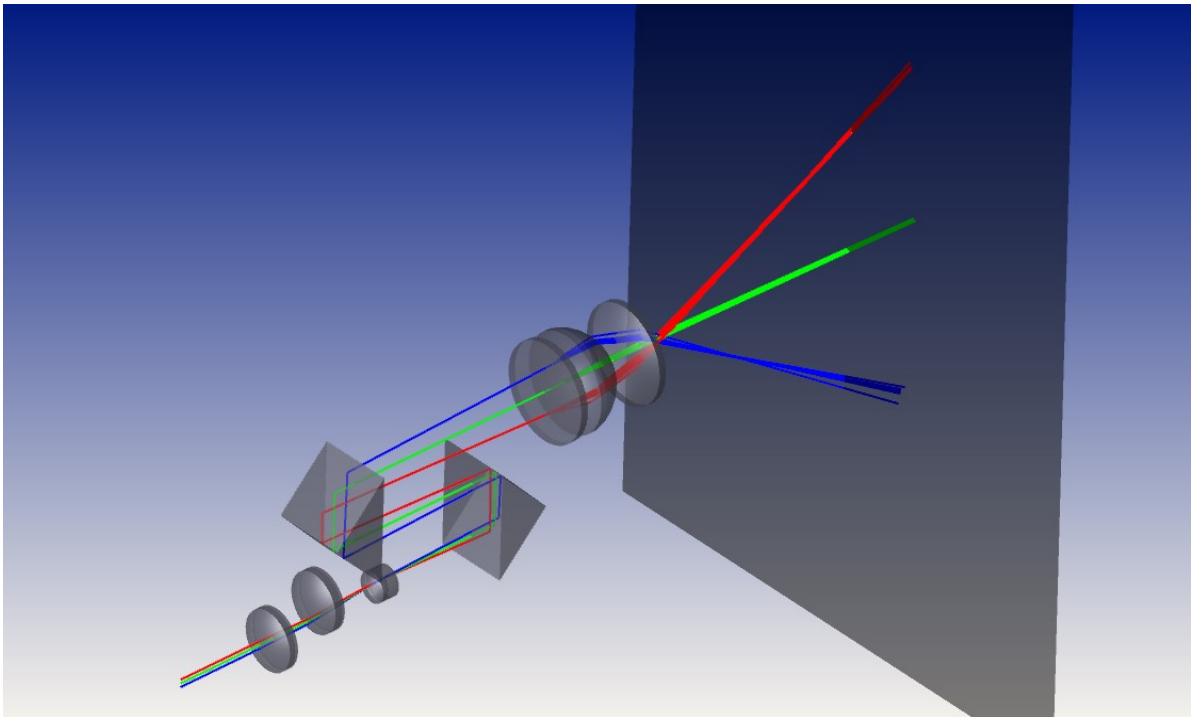

Figure 3.21 3-D shaded model for Case 3

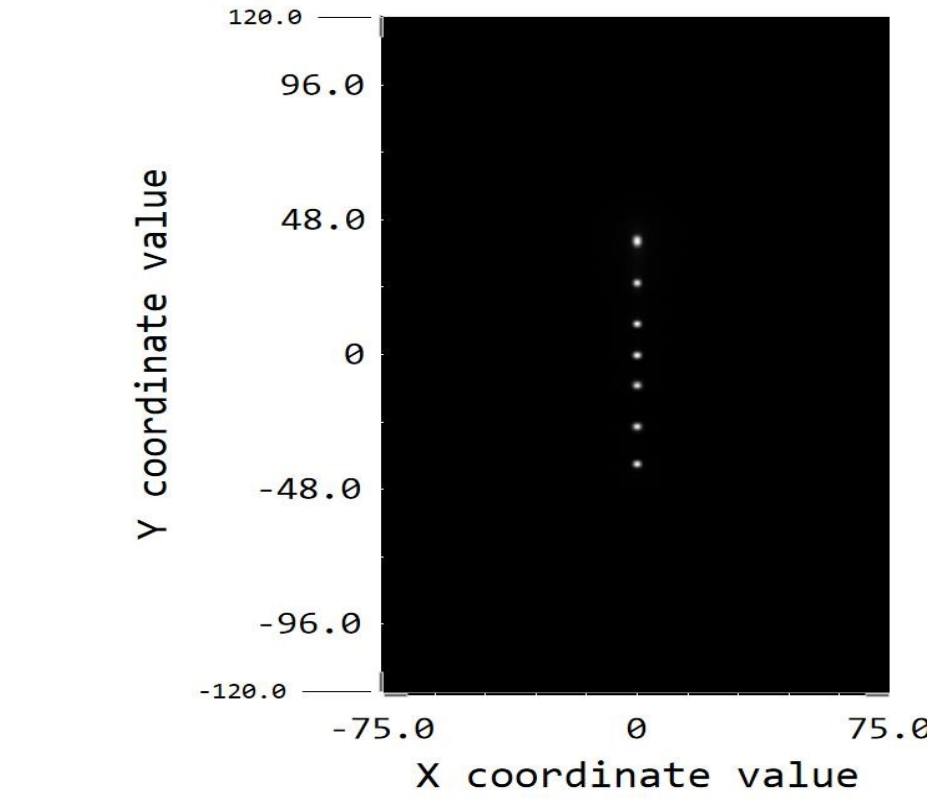

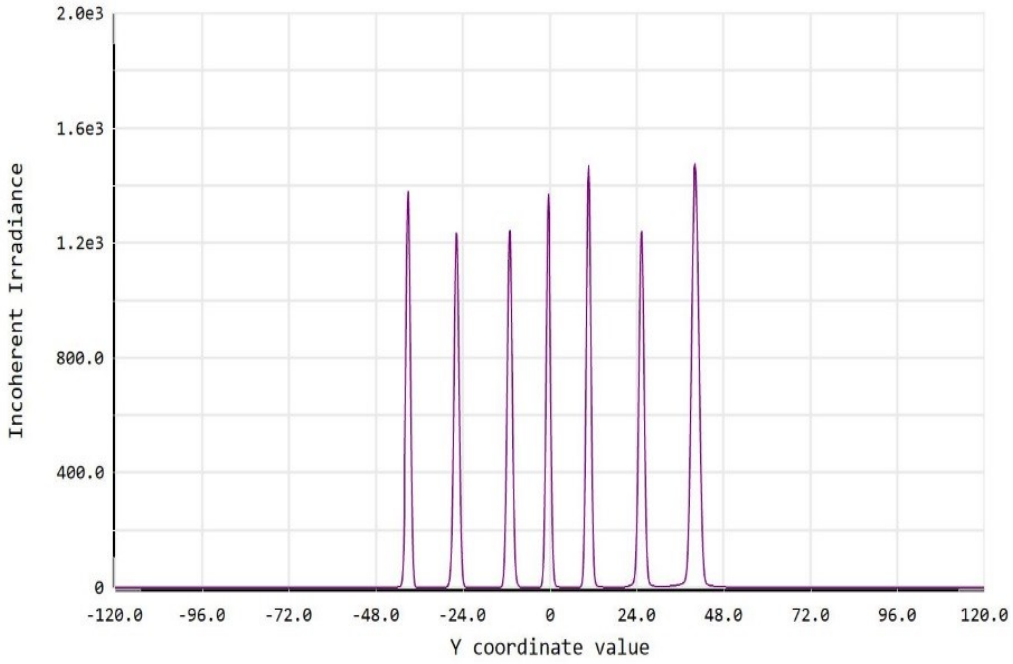

Figure 3.202 Ray trace results for Case 3

3.4.4 CASE 4

Case 4 was simulated by adding another prism to the design of Case 3 to further increase the path length and subsequently, the scan angle. The figure below shows the design layout.

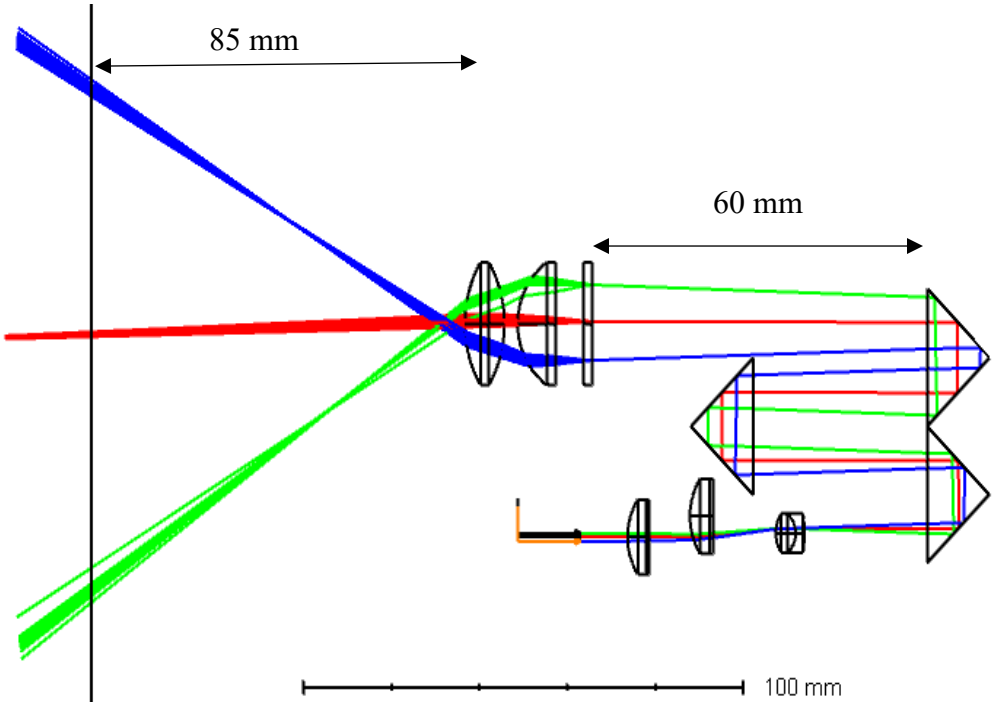

Figure 3.213 3D layout for Case 4

The results of the ray trace are shown in figure 3.24 below. Even though addition of a third prism leads to an increase in path length, the corresponding scan angle is only increased to 60°. This is due to the fact that not all values of focal length of the tunable lenses could be used in this design, as using higher values of focal length caused the rays to rays to take unwanted paths and reflect among the prisms instead of reaching the optical diffuser. Thus, a lower range of focal length values used lead to a lower range of scan angle than expected.

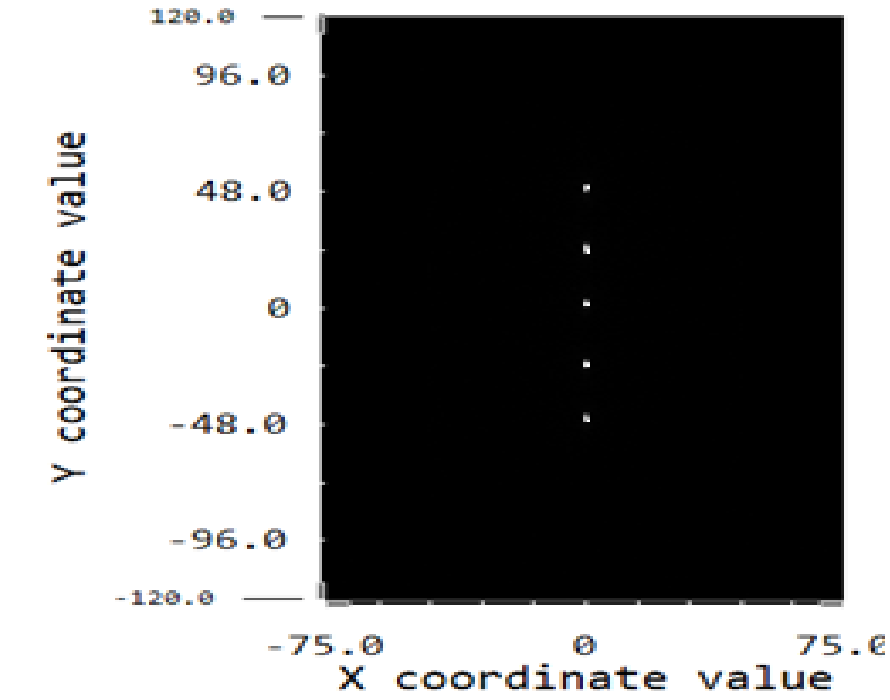

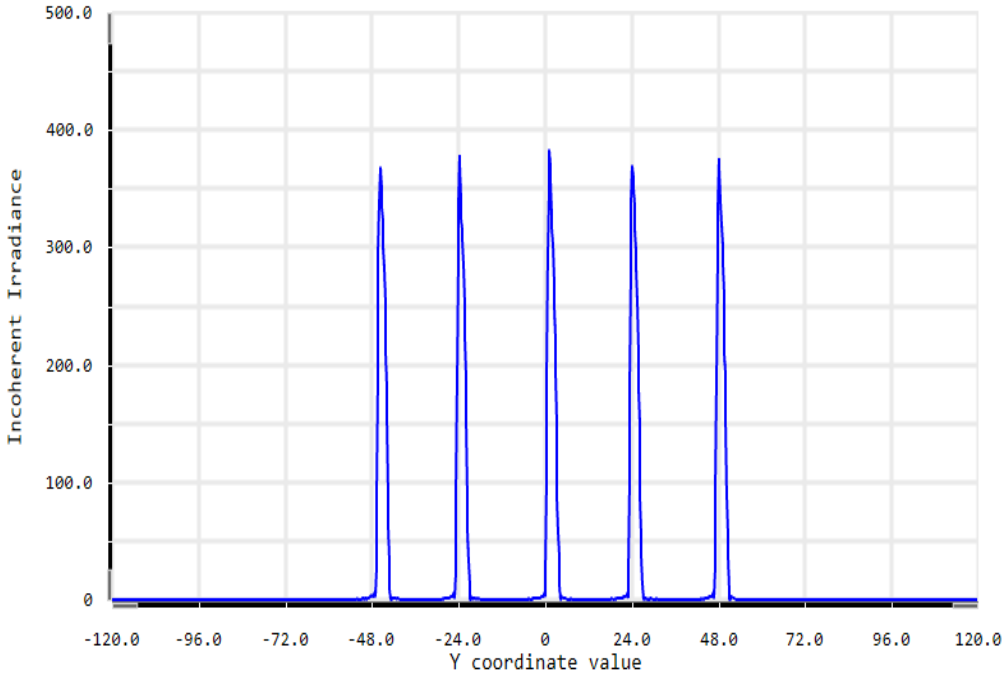

Figure 3.224 Ray trace results for Case 4

3.5 COMPARISON OF SIZE, SCAN ANGLE AND BEAM DIVERGENCE

3.5.1 COMPARING THE PHYSICAL LENGTH VS OPTICAL PATH LENGTH

Figure 3.25 below compares the distance between the relay lens and the diffuser of the first and the final design. In the first design, the physical length between them is 280 mm which is the same length as the optical path. In the final design, the physical distance between the relay lens and the diffuser is only 48 mm. The total optical path length, however, is the sum of the path length travelled between the two prisms, as calculated in section 3.3.3 and the distance between the second prism and the diffuser. Therefore, the total distance the rays travel between the relay lens and the diffuser is:

$$\Delta = 164 + 60 = 224\ mm$$

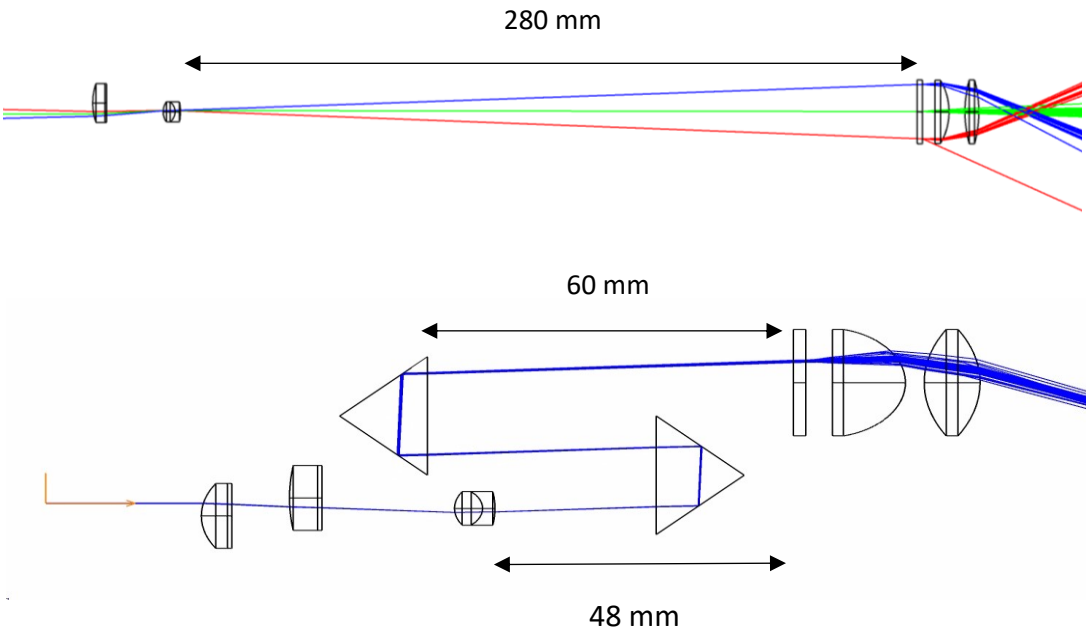

Figure 3.235 Comparing the optical path length and the physical length between the relay lens and the diffuser in Case 1 and Case 3

To further demonstrate the effect of the prisms replacing the optical path, the 280 mm path length in Case 1, with all its specifications kept constant, was replaced with prisms to compare the value of the angle vs the optical path length. The two tunable lenses were placed 41mm apart, the relay lens was placed 22 mm away and 50 mm objective lenses were used, same as Case 1.

The figures below show three cases, where the diffuser and objective lenses were placed at different distances from the prism arrangement making the total path length 224, 254 and 280 mm respectively. Varying the distance between the diffuser and the prism and increasing the path length led to increasing scan angles. The results are shown in figure 3.27. The first figure shows the scan for a path length of 224 mm from which the scan angle is calculated as 31°, the path length of 254 mm corresponds with an angle of 50° and a path length of 280mm corresponds with an angle of 76°. The first result with a path length of 224 mm shows the same results as replacing the objective lenses in Case 3 (which also had a path length of 224mm) with 50 mm objective lenses, as shown in the next section. This indicates that reducing the distance between the tunable lenses, and relay lens does not affect the scan angle.

The third result, where 280mm was created with prisms instead of a direct path between the relay lens and the diffuser, indicates the same scan angle as Case 1. This indicates that replacing the optical path with rectangular prisms has no effect on the angle, and the only effect is reducing the length of the device.

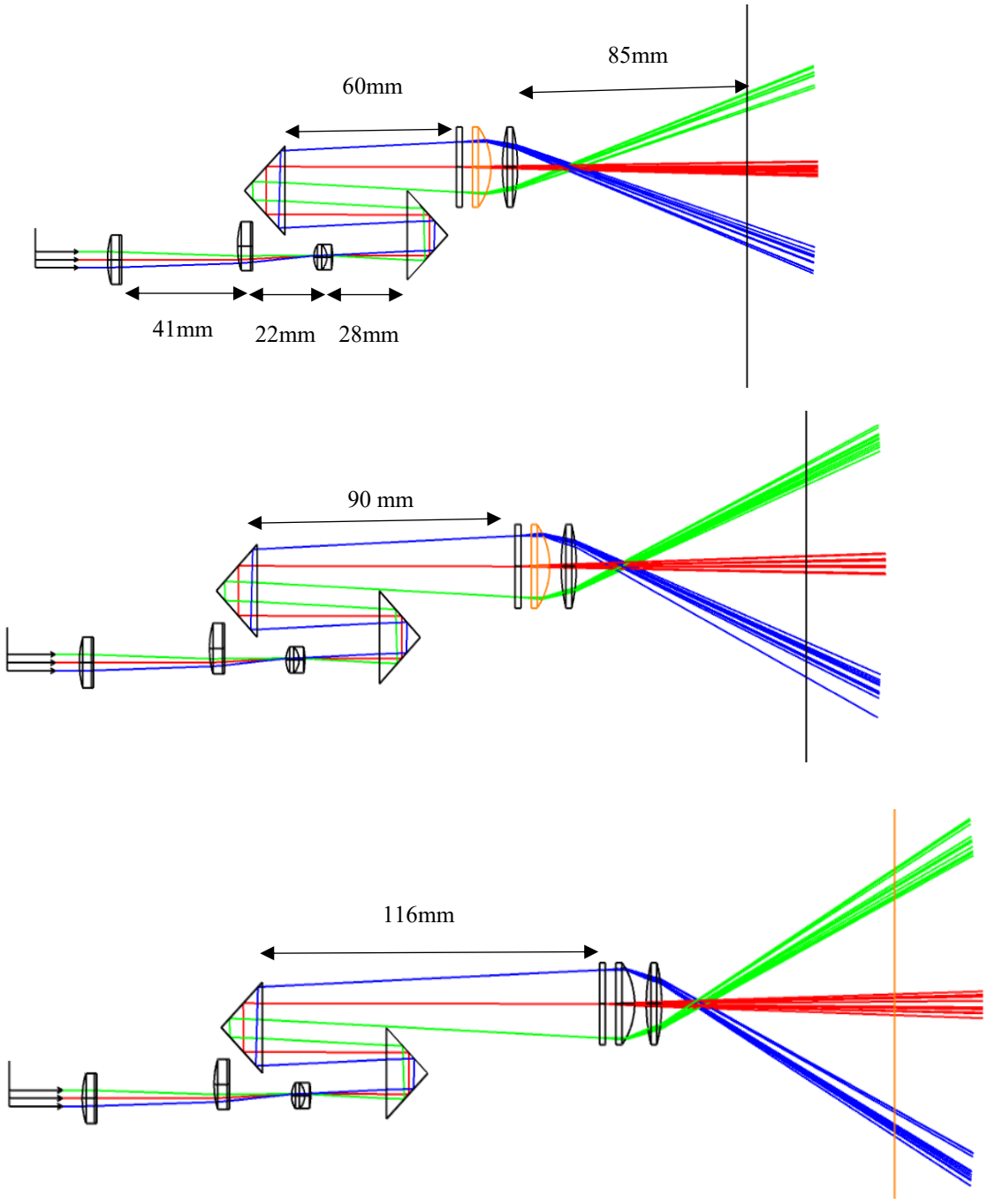

Figure 3.246 Demonstration of the effect of adding prisms on the optical path length and the scan angle

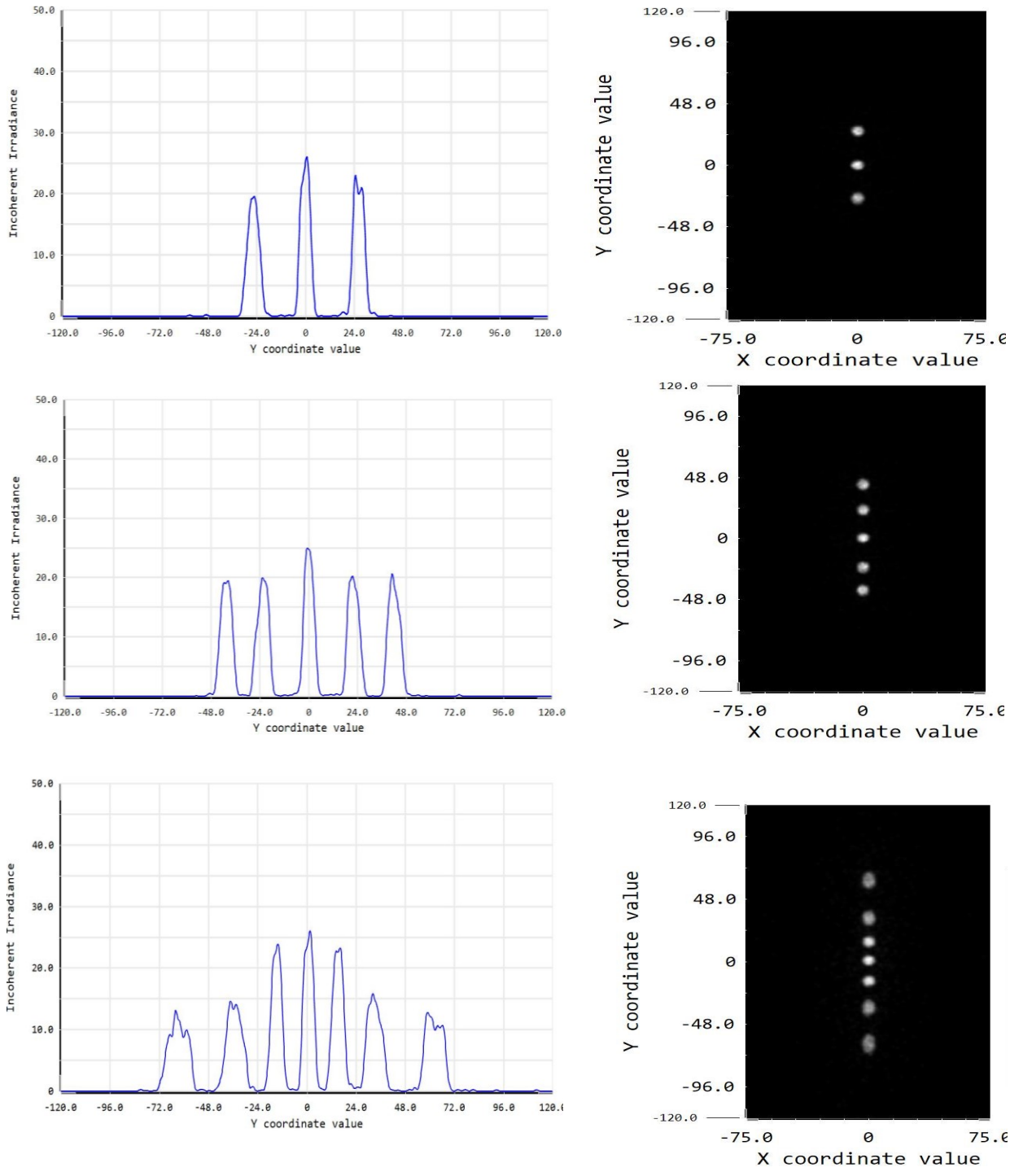

Figure 3.257 Results from Figure 3.26 above

3.5.2 COMPARING BEAM DIVERGENCE USING 50 MM AND 25 MM OBJECTIVE LENSES

Figure 3.28 below demonstrates the effect of using 50 mm focal length objective lenses vs 25mm objective lenses. The first set of ray trace shows the result obtained from using 50 mm objective lenses on the design in case 3, and the second set shows the result of using 25 mm lenses on the same design. Not only is the scan wider for the second case and reaching farther points along y-axis, but the beam size is also visibly smaller.

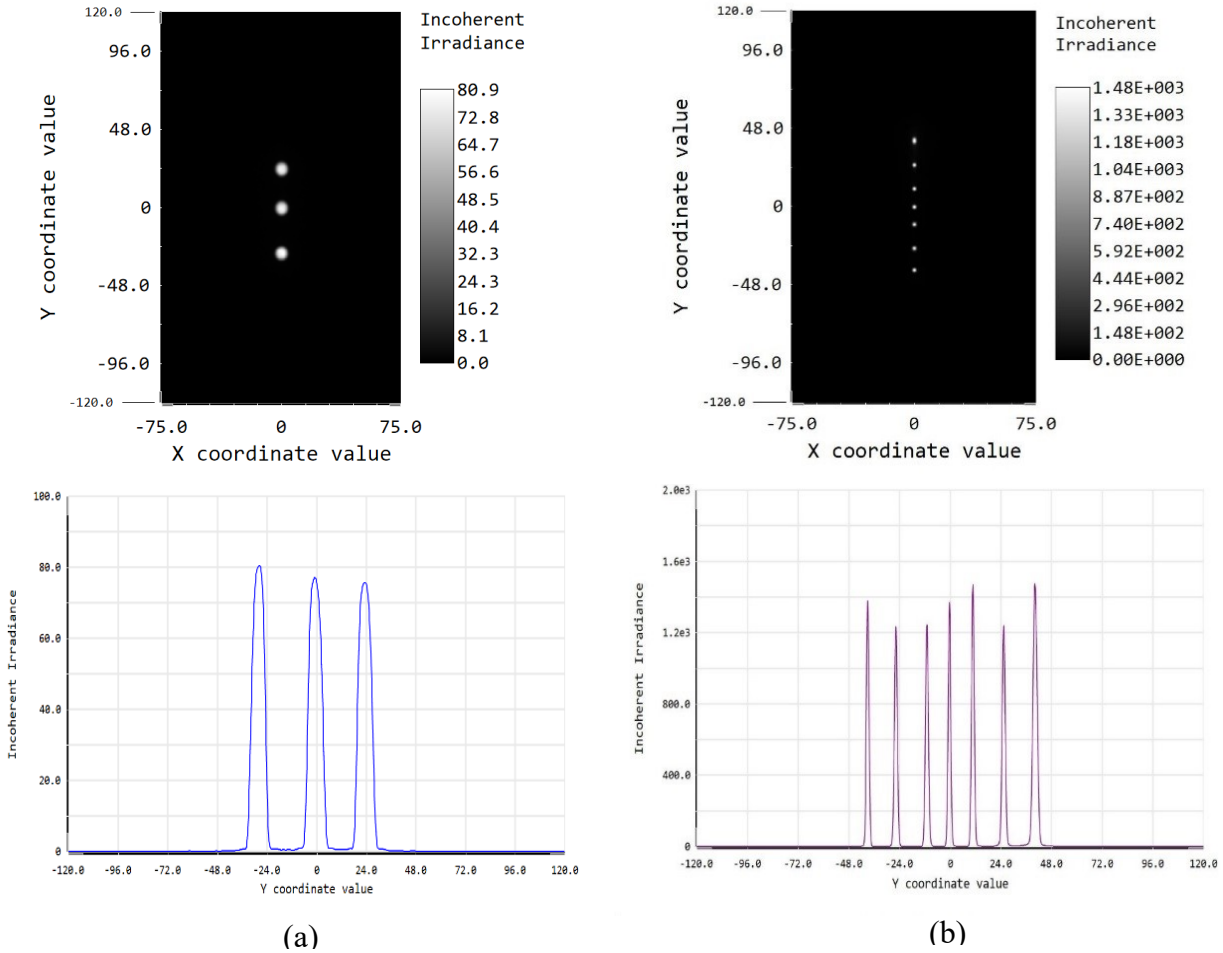

(a) (b)

Figure 3.268 Two sets of ray traces (a) using 50 mm objective lenses and (b) using 25 mm objective lenses

The RMS spot size of the beam in the two cases is calculated using Zemax. For the first case using 50 mm objective lenses, the RMS spot size when the detector is placed 85 mm from the design is found to be 6.84 mm. And when the detector is moved to 2m away, the RMS spot size increases to 43 mm due to divergence.

In contrast, when using 25mm objective lenses, the RMS spot radius is 1.82 mm when the detector is placed 85 mm from the design and expands to 15 mm when the detector is placed 2 m away.

The RMS beam radius vs the distance of the detector from the device is plotted in figure 3.29 below to demonstrate the beam divergence for the two focal lengths. The red line indicates the values gotten from using a 50 mm lens and the blue line indicated values achieved from using a 25 mm lens.

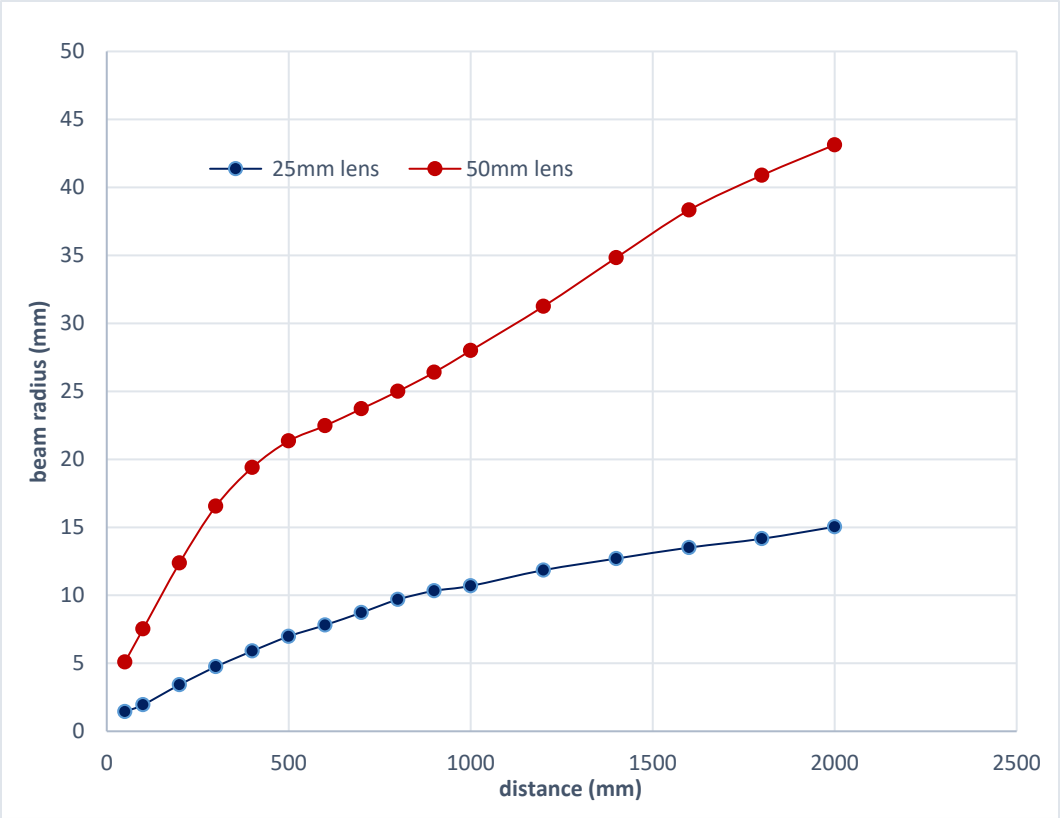

Figure 3.279 Beam RMS spot radius vs distance from the device

It can be seen from the greater slope of the red line that the beam increases in size much more rapidly. The blue line has a smaller slope indicating a more collimated beam which is more suitable for LIDAR applications.

The beam divergence can be calculated for the two models using the beam radius at two different points away from the origin and the distance between them. Let R_1 and R_2 be the radii of the beam at two different positions, and L be the distance between them. Then the beam divergence θ is then given by:

$$\theta = 2\tan^{-1}\left(\frac{R_2 - R_1}{2L}\right)$$

Using this formula, the beam divergence for case 3 was found to be 0.45° whereas for case 1 and case 2 it is 1.73°.

Table 3.2 below summarizes the result from the three designs. In terms of the longitudinal size of the device, there is a significant reduction in the latter two designs from the original one. The change is length between the latter two designs is not very significant, as the third design is only 5mm longer than the second one. On the other hand, the total length of the original device is 385mm while the total length of the final device is 119 mm. This corresponds to a 69% reduction in the length of the device.

Regarding the scan angle, the original device had a higher scan range of 76°. When the optical path length was reduced in the second model, this scan range dropped to only 16°. Meanwhile the use of prisms to fold the path of light led to an increase in the scan angle to 52°.

Case	1	2	3	4
Total length (mm)	385	114	119	125
Total scan angle	76°	16°	52°	60°
Beam divergence	1.73°	1.73°	0.45°	0.45°

Table 3.2 Summary of results

When comparing the reduction in length vs the scan angle between the first and the last model, the length is reduced by 69% in the last model. The beam divergence is also reduced by 74%.

3.5.3 EFFECT OF REFLECTION ON THE TOTAL TRANSMITTED POWER

The effects of reflection in the optical components used will affect the efficiency of the system. The table below lists the percentage transmission of each optical component at 905 nm wavelength, assuming all components are coated with anti-reflection coating. [12][50][51][52][53][54]

Optical component	Transmission at 905 nm with AR coating (%)
Tunable lens	94.6
Achromatic doublet lens	99.8
90° prism	99.6
Optical diffuser	80
Plano convex lens	99.5
Bi convex lens	99.5

Table 3.3 Percentage transmission of each component at 905 nm wavelength of light

Thus, for Case 3 which uses each of these components, 70% of the power transmitted from the laser will be transmitted through the device. Whereas 69.7% of the power will be transmitted for Case 4 which uses an additional prism.

4. CONCLUSION

4.1 THESIS CONCLUSION

Even though the technology behind LIDAR has been around for many years now, recently there has been a great deal of research on the topic. Improvements are made on all components of the device making it suitable for different applications. One of the reasons LIDAR has gained so much focus recently is its importance in detection systems for autonomous vehicles. Autonomous vehicles have seen significant improvements recently with major companies around the world all working towards making them accessible and safe to use for everyone. But even with all the developments in this area, autonomous vehicles are still far from being efficient enough for everyday use, cheap enough to be ubiquitous, or safe enough to be driven without a human controller present. There is still room for lots of improvements to be made in terms of obstacle detection, like improvements in accuracy of distance measurement, image resolution, detection speed, or response speed. Improvements are also essential in making the vehicle itself and the components of the vehicle more efficient and cost-effective so that autonomous vehicles can be made available to everyone. And for this reason, LIDAR devices need to be cheaper and more efficient that can capture surrounding images at high resolution.

The mechanical gear used in LIDAR to steer laser beams are the main reason behind their high cost, and consequently the high cost of self-driving cars. It also makes the LIDAR device bulky and heavy. The aim of this thesis was to create a non-mechanical system for steering laser beams which can be used specifically in applications for LIDAR devices in self-driving cars. The system made use of focus tunable lenses, which uses electrical current to exert pressure on a container of optical fluid, thereby changing the focal length of the lens. This change in focal length resulted in

shifting the position of the beam when two lenses are used one after the other. Other optical components, like achromatic doublet lens, optical diffuser, and objective lenses were used after the tunable lenses to focus the beam and increase the angle of the scan. Finally, 90° prisms were used to fold the optical path to make the device more compact.

Three different design stages were carried out with the goal of improving the scan angle, reducing the longitudinal size, and reducing the beam divergence.

1. In the first design, the two tunable lenses were placed 41mm apart with the relay lens positioned 22 mm from the second tunable lens to focus the beam onto an optical diffuser 280 mm away. The diffuser was followed by a plano-convex and a bi-convex objective lens of 50mm focal length. The entire device was about 385mm long and the total scan angle was 76°. The beam divergence was calculated to be 1.73°.
2. The second design aimed at finding the effect of reducing the length between the relay lens and the diffuser. Therefore, the length between the relay lens and the diffuser was reduced from 280 mm to 55mm. The distance between the two tunable lenses was also reduced to 10 mm followed by the relay lens 12 mm away. The total length of the device was reduced to just 114 mm, but consequently the total scan angle was also reduced to only 16°. The beam divergence was the same as before at 1.73°.
3. In the third design, instead of removing the optical path between the relay lens and the diffuser all together, it was replaced with prisms so the light would reflect along the walls of the prism, and travel in a folded path and therefore reduce the longitudinal size of the device. Two prisms were used, and the light rays underwent total internal reflection a total of four times and were then focused onto the diffuser. The arrangement of the prisms made the total path travelled by the light to be 164 mm, and with the diffuser placed 60 mm away

from the last prism, the total optical path length was 224 mm. This is still lower than the path length in case 1 where the path length was 280 mm but increasing it any more would result in a larger setup where our goal is to make the device as compact as possible. The device size was reduced to 119 mm, and there was a reduction in scan angle which in this case is 52°. But this angle is still high enough for practical applications.

Another change made in this design was that the focal length of the objective lenses used after the diffuser were reduced from 50mm to 25mm. This not only increased the scan angle compared to the second design, but it also resulted in an output beam with significantly lower divergence angle of only 0.45°.

4. An additional prism was added in the fourth case in an effort to further increase the optical path length and the angle. Even though the angle increased to 60°, this increase does not correspond fully with the increase in the optical path. This is because the full range of focal lengths could not be used in this design, as increasing it beyond a certain value caused the rays to take unwanted paths and not reach the diffuser.

Comparing the final design of the system with the first one, we can see that there is a 69% reduction in size with a significant 74% reduction in the beam divergence. Losses due to reflection in the components was also considered, indicating a 70% efficiency and 905nm.

4.2 FUTURE WORK

Future work related to this thesis can look at a number of factors for improvement including:

1. The scan angle may be further increased by adding more prisms to increase the optical path of the light.
2. Improvements can be made in increasing the speed of steering the light beam.

REFERENCES

[1] C. V. P. and M. R. Watts, "MIT and DARPA Pack LIDAR Sensor onto Single Chip," *IEEE Spectrum: Technology, Engineering, and Science News*, 04-Aug-2016. [Online]. Available: https://spectrum.ieee.org/tech-talk/semiconductors/optoelectronics/mit-LIDAR - on-a-chip. [Accessed: 07-Jun-2018].

[2] J. C. Hulme *et al.*, "Fully integrated hybrid silicon two-dimensional beam scanner," *Opt. Express, OE*, vol. 23, no. 5, pp. 5861–5874, Mar. 2015.

[3] B. Smith, B. Hellman, A. Gin, A. Espinoza, and Y. Takashima, "Single chip LIDAR with discrete beam steering by digital micromirror device," *Opt. Express, OE*, vol. 25, no. 13, pp. 14732–14745, Jun. 2017.

[4] C. T. DeRose *et al.*, "Electronically controlled optical beam-steering by an active phased array of metallic nanoantennas," *Opt. Express, OE*, vol. 21, no. 4, pp. 5198–5208, Feb. 2013.

[5] M. Zohrabi, R. H. Cormack, and J. T. Gopinath, "Wide-angle nonmechanical beam steering using liquid lenses," *Opt. Express, OE*, vol. 24, no. 21, pp. 23798–23809, Oct. 2016.

[6] J. Kim, M. N. Miskiewicz, S. Serati, and M. J. Escuti, "Nonmechanical Laser Beam Steering Based on Polymer Polarization Gratings: Design Optimization and Demonstration," *Journal of Lightwave Technology*, vol. 33, no. 10, pp. 2068–2077, May 2015.

[7] M. T. Johnson, D. F. Siriani, M. P. Tan, and K. D. Choquette, "High-Speed Beam Steering with Phased Vertical Cavity Laser Arrays," *IEEE Journal of Selected Topics in Quantum Electronics*, vol. 19, no. 4, pp. 1701006–1701006, Jul. 2013.

[8] B. Ashrafi-Nia, L. Yousefi, and M. Shahabadi, "Optical beam-steering using a hybrid plasmonic Rotman lens," in *2014 Third Conference on Millimeter-Wave and Terahertz Technologies (MMWATT)*, 2014, pp. 1–4.

[9] A. Kilpela, "Pulsed time-of-flight laser range finder techniques for fast, high precision measurement applications," *ResearchGate*, Jan. 2004.

[10] Yaacobi, J. Sun, M. Moresco, G. Leake, D. Coolbaugh, and M. R. Watts, "Integrated phased array for wide-angle beam steering," *Opt. Lett., OL*, vol. 39, no. 15, pp. 4575–4578, Aug. 2014.

[11] "Optotune Focus Tunable Lens Brochure," *Optotune Downloads*. [Online]. Available: https://www.optotune.com/downloads2. [Accessed: 20-Jul-2018].

[12] "Datasheet: EL-10-30-Series Fast Electrically Tunable Lens," *Optotune Downloads*, 2017. [Online]. Available: https://www.optotune.com/downloads. [Accessed: 29-Aug-2018].

[13] "Electrical lens EL-10-30-TC." [Online]. Available: https://www.optotune.com/products/focus-tunable-lenses/electrical-lens-el-10-30. [Accessed: 11-Oct-2018].

[14] "How does LIDAR work? The science behind the technology," *LIDAR UK*. [Online]. Available: http://www.LIDAR -uk.com/how-LIDAR -works/. [Accessed: 02-Sep-2018].

[15] S. Liu, L. Li, J. Tang, S. Wu, and J.-L. Gaudiot, "Creating Autonomous Vehicle Systems," *Synthesis Lectures on Computer Science*, vol. 6, no. 1, p. i-186, Oct. 2017.

[16] V. Poulton *et al.*, "Coherent solid-state LIDAR with silicon photonic optical phased arrays," *Opt. Lett., OL*, vol. 42, no. 20, pp. 4091–4094, Oct. 2017.

[17] A. Arora, "Zemax OpticStudio Knowledgebase - Zemax," *Exploring Non-Sequential Mode in OpticStudio*, 08-Oct-2014. [Online]. Available: https://customers.zemax.com/os/resources/learn/knowledgebase/exploring-non-sequential-mode-in-zemax. [Accessed: 29-Aug-2018].

[18] "Why Use an Achromatic Lens?" *Edmund Optics*. [Online]. Available: https://www.edmundoptics.com/resources/application-notes/optics/why-use-an-achromatic-lens/. [Accessed: 27-Sep-2018].

[19] G. M. Gehring, H. Shin, R. W. Boyd, C.-M. Kim, and B. S. Ham, "Tunable Optical Time Delay of Quantum Signals Using a Prism Pair," *Opt. Express, OE*, vol. 18, no. 18, pp. 19156–19162, Aug. 2010.

[20] "Binoculars - How Binoculars Work?" *AZo Optics*, 07-Mar-2008. [Online]. Available: https://www.azooptics.com/Article.aspx?ArticleID=142. [Accessed: 27-Sep-2018].

[21] W. J. Walecki and P. Walecki, "Robust diffuser and roughness metrology tool for LED manufacturing," *ResearchGate*, Mar. 2015.

[22] J. Hecht, “LIDAR for Self-Driving Cars,” *Optics & Photonics News, OPN*, vol. 29, no. 1, pp. 26–33, Jan. 2018.

[23] M. Nicholson, “How to Use the Stock Lens Matching Tool,” Zemax OpticStudio Knowledgebase - Zemax, 23-Dec-2015. [Online]. Available: https://customers.zemax.com/os/resources/learn/knowledgebase/how-to-use-the-stock-lens-matching-tool. [Accessed: 01-Nov-2018].

[24] Davies, “Inside the Races That Jump-Started the Self-Driving Car,” *Wired*, 10-Nov-2017.

[25] “Journey – Waymo.” [Online]. Available: https://waymo.com/journey/. [Accessed: 16-Sep-2018].

[26] M. Lapedus, “Radar versus LIDAR,” *Semiconductor Engineering*, Oct-2017.

[27] “Radar Basics - Phased Array Antenna,” *Radar Tutorial*. [Online]. Available: http://www.radartutorial.eu/06.antennas/Phased%20Array%20Antenna.en.html. [Accessed: 27-Sep-2018].

[28] P. F. McManamon *et al.*, “Optical phased array technology,” *Proceedings of the IEEE*, vol. 84, no. 2, pp. 268–298, Feb. 1996.

[29] N. Hutchison *et al.*, “High-resolution aliasing-free optical beam steering,” *Optica, OPTICA*, vol. 3, no. 8, pp. 887–890, Aug. 2016.

[30] H. W. Yoo *et al.*, "MEMS-based LIDAR for autonomous driving," *Elektrotech. Inftech.* Jul. 2018.

[31] H. V. Heeren and P. Salomon, "MEMS Recent Developments, Future Directions." 2007.

[32] Time-of-Flight vs. Phase-Based Laser Scanners: Right Tool for the Job," *SPAR 3-D*, 22-Jun-2004. [Online]. Available: https://www.spar3-D.com/news/related-new-technologies/time-of-flight-vs-phase-based-laser-scanners-right-tool-for-the-job/. [Accessed: 23-Sep-2018].

[33] P. McManamon, *Field Guide to LIDAR*. SPIE, 2015.

[34] "LIDAR: Automatic Driving from the Perspective of Photoelectricity Technology." [Online].
Available: http://mp.weixin.qq.com/s?__biz=MzI2NDI4MTY3OA==&mid=2247485510&idx=1&sn=00c3155088a8a16fbf3bdfcbcbff4f9c&chksm=eaae4367ddd9ca71af720e8d0536d49c6fcb0812-D9ba446551b0041a2990047c3632-Dbd6649c&mpshare=1&scene=23&srcid=0324KRQ49C16xzYFsJ2Z2-DpX&lan=en#rd [Accessed: 09-Apr-2018].

[35] A. Kukko, "Mobile laser scanning - system development, performance and applications" Aalto University School of Engineering, 2013.

[36] "Lasers for LIDAR: Application parameters dictate laser source selection in LIDAR systems." [Online]. Available: https://www.laserfocusworld.com/articles/print/volume-53/issue-03/features/lasers-for-LIDAR -application-parameters-dictate-laser-source-selection-in-LIDAR -systems.html. [Accessed: 06-Jun-2018].

[37] "Technology – Analog Photonics," *Silicon Photonics*. [Online]. Available: http://www.analogphotonics.com/technology/. [Accessed: 27-Sep-2018].

[38] T. B. Lee, "Why experts believe cheaper, better LIDAR is right around the corner," Ars Technica, 01-Jan-2018. [Online]. Available: https://arstechnica.com/cars/2018/01/driving-around-without-a-driver-LIDAR -technology-explained/. [Accessed: 07-Jun-2018].

[39] M. Macias, "New Technology: Self Driving Cars and More," *Air light sport*.

[40] D. Muoio, "These 19 companies are racing to build self-driving cars in the next 5 years," Business Insider. [Online]. Available: https://www.businessinsider.com/companies-making-driverless-cars-by-2020-2017-1. [Accessed: 09-Oct-2018].

[41] "MEMS Mirrors," *Mirrorcle Technologies, Inc. - Devices*. [Online]. Available: https://mirrorcletech.com/devices.html. [Accessed: 09-Oct-2018].

[42] "Lidar Sensors - Infineon Technologies." [Online]. Available: https://www.infineon.com/cms/en/product/sensor/lidar-sensors/. [Accessed: 10-Oct-2018].

[43] E. Guizzo, "How Google's Self-Driving Car Works," *IEEE Spectrum: Technology, Engineering, and Science News*, 18-Oct-2011. [Online]. Available: https://spectrum.ieee.org/automaton/robotics/artificial-intelligence/how-google-self-driving-car-works. [Accessed: 07-Jun-2018].

[44] P. Olivier, "Leddar Optical Time-of-Flight Sensing Technology: A New approach to Detection and Ranging," LeddarTech Inc., 2016.

[45] U. Hofmann *et al.*, "Resonant biaxial 7-mm MEMS mirror for omnidirectional scanning," vol. 13, pp. 011103-13–9, 2013.

[46] Zemax LLC, *How to Use Luminit's LSD Model in OpticStudio*. 2016.

[47] Zemax LLC, *Creating sequential systems with prisms, CAD parts, and other complex objects in OpticStudio*. 2017.

[48] "HDL-64E Datasheet," 2018. [Online]. Available: https://www.velodynelidar.com/downloads.html. [Accessed: 08-Nov-2018].

[49] "LASER Safety in a LiDAR World," Velodyne LiDAR, 03-May-2017.

[50] "Mounted Achromatic Doublets, AR Coated: 650 - 1050 nm." [Online]. Available: https://www.thorlabs.com/newgrouppage9.cfm?objectgroup_id=3647. [Accessed: 12-Jan-2019].

[51] "AR-Coated, N-BK7 Ground Glass Diffusers." [Online]. Available: https://www.thorlabs.com/NewGroupPage9.cfm?ObjectGroup_ID=6901. [Accessed: 12-Jan-2019].

[52] "Right-Angle Prisms." [Online]. Available: https://www.thorlabs.com/newgrouppage9.cfm?objectgroup_id=142. [Accessed: 12-Jan-2019].

[53] "N-BK7 Plano-Convex Lenses (AR Coating: 650-1050 nm)." [Online]. Available: https://www.thorlabs.com/newgrouppage9.cfm?objectgroup_id=3280. [Accessed: 12-Jan-2019].

[54] "Mounted N-BK7 Bi-Convex Lenses (AR Coating: 650 - 1050 nm)." [Online]. Available: https://www.thorlabs.com/newgrouppage9.cfm?objectgroup_id=9384. [Accessed: 12-Jan-2019].